Cellular/Molecular

Distinct P2Y Receptors Mediate Extension and Retraction of Microglial Processes in Epileptic and Peritumoral Human Tissue

Giampaolo Milior,[1,2] Mélanie Morin-Brureau,[1] Farah Chali,[1] Caroline Le Duigou,[1] Etienne Savary,[1] Gilles Huberfeld,[2,3] Nathalie Rouach,[2] Johan Pallud,[4] Laurent Capelle,[6] Vincent Navarro,[5] Bertrand Mathon,[6] Stéphane Clemenceau,[6] and Richard Miles[1]

[1]Cortex and Epilepsie, Institut National de la Santé et de la Recherche Médicale U1127, Centre National de la Recherche Scientifique Unité Mixte de Recherche 7225, Université Pierre et Marie Curie, Université Paris 6, Institut du Cerveau et de la Moelle épinière, Paris 75013, France, [2]Neuroglial Interactions in Cerebral Physiopathology, Center for Interdisciplinary Research in Biology, Collège de France, Centre National de la Recherche Unité Mixte de Recherche 7241, Institut National de la Santé et de la Recherche Médicale U1050, Labex Memolife, PSL Research University, Paris 75005, France, [3]Clinical Neurophysiology Department, Université Pierre et Marie Curie, Université Paris 6, Hopital Pitié-Salpêtrière, AP-HP, Paris 75013, France, [4]Neurochirurgie, Hôpital Sainte-Anne, Paris Descartes University, IMA-BRAIN, Institut National de la Santé et de la Recherche Médicale, U894 Centre de Psychiatrie et Neurosciences, Paris 75014, France, [5]Epilepsy Unit, and [6]Neurochirurgie, AP-HP, Hôpital Pitie-Salpêtrière, Paris 75013, France

Microglia exhibit multiple, phenotype-dependent motility patterns often triggered by purinergic stimuli. However, little data exist on motility of human microglia in pathological situations. Here we examine motility of microglia stained with a fluorescent lectin in tissue slices from female and male epileptic patients diagnosed with mesial temporal lobe epilepsy or cortical glioma (peritumoral cortex). Microglial shape varied from ramified to amoeboid cells predominantly in regions of high neuronal loss or closer to a tumor. Live imaging revealed unstimulated or purine-induced microglial motilities, including surveillance movements, membrane ruffling, and process extension or retraction. At different concentrations, ADP triggered opposing motilities. Low doses triggered process extension. It was suppressed by P2Y12 receptor antagonists, which also reduced process length and surveillance movements. Higher purine doses caused process retraction and membrane ruffling, which were blocked by joint application of P2Y1 and P2Y13 receptor antagonists. Purinergic effects on motility were similar for all microglia tested. Both amoeboid and ramified cells from mesial temporal lobe epilepsy or peritumoral cortex tissue expressed P2Y12 receptors. A minority of microglia expressed the adenosine A2A receptor, which has been linked with process withdrawal of rodent cells. Laser-mediated tissue damage let us test the functional significance of these effects. Moderate damage induced microglial process extension, which was blocked by P2Y12 receptor antagonists. Overall, the purine-induced motility of human microglia in epileptic tissue is similar to that of rodent microglia in that the P2Y12 receptor initiates process extension. It differs in that retraction is triggered by joint activation of P2Y1/P2Y13 receptors.

Key words: **acute human tissue; G-protein-coupled receptors; human microglia; live imaging; microglial motility**

Significance Statement

Microglial cells are brain-resident immune cells with multiple functions in healthy or diseased brains. These diverse functions are associated with distinct phenotypes, including different microglial shapes. In the rodent, purinergic signaling is associated with changes in cell shape, such as process extension toward tissue damage. However, there are little data on living human microglia, especially in diseased states. We developed a reliable technique to stain microglia from epileptic and glioma patients to examine responses to purines. Low-intensity purinergic stimuli induced process extension, as in rodents. In contrast, high-intensity stimuli triggered a process withdrawal mediated by both P2Y1 and P2Y13 receptors. P2Y1/P2Y13 receptor activation has not previously been linked to microglial morphological changes.

Introduction

Microglia are brain-resident immune cells with multiple functional phenotypes. In healthy tissue, ramified microglial processes move constantly to surveil the space around them (Dailey and Waite, 1999; Davalos et al., 2005; Nimmerjahn et al., 2005). During development, microglia remove superfluous synapses and cells to shape neuronal connectivity (Paolicelli et al., 2011; Schafer et al., 2012). In response to damage, microglial processes extend toward a site of injury and phagocytose cellular debris (Koizumi et al., 2007). In many pathologies, microglia liberate inflammatory mediators (Sanz and Di Virgilio, 2000; Bianco et al., 2005), but they also engage in repair and resolution (Raposo and Schwartz, 2014).

Distinct microglial phenotypes (Streit et al., 1988) depend in part on signaling mediated by purinergic receptors (Hanisch and Kettenmann, 2007). Purines are released depending on neuronal activity and cell damage (Dale and Frenguelli, 2009). They act on ionotropic P2X receptors (Khakh and North, 2012), on G-protein-coupled P2Y receptors (von Kügelgen, 2006), and on adenosine receptors expressed by microglia (Chen et al., 2014). Distinct microglial phenotypes have been linked with activation of different purinergic receptors. Extension of processes toward an injury is mediated via P2Y12 receptors (Honda et al., 2001; Haynes et al., 2006). P2Y6 receptors trigger phagocytosis (Koizumi et al., 2007) and P2X7 receptors activate inflammasome processing of cytokines for secretion (Pelegrin et al., 2008).

Responses to purinergic stimuli differ for microglia in an inflammatory context and those in a healthy brain. While healthy cells extend processes toward a purine source or cell damage (Davalos et al., 2005; Haynes et al., 2006), processes of microglia in an inflamed brain retract. This difference has been attributed to a switch in receptor expression from P2Y12 to adenosine A2A receptors (Orr et al., 2009; Gyoneva et al., 2014). However, motility patterns induced by purinergic stimulation have rarely been studied for human microglia in a pathological or inflammatory context.

We therefore examined the effects of purines on motility in microglia of tissue from patients with medial temporal lobe epilepsies and with epileptic cortical tissue surrounding or infiltrated by gliomas. A fluorescent lectin (Bordey and Spencer, 2003; Schwendele et al., 2012) was used to label microglia, enabling 2-photon imaging of living cells over several hours. In the absence of stimulation, microglia varied from round cells, through microglia with few processes to highly ramified cells (Boche et al., 2013; Morin-Brureau et al., 2018). We found that purinergic stimuli induced distinct and opposing motility responses: extension at low doses and retraction of processes at higher doses. Our data suggest that extension was dependent on activation of P2Y12 receptors as in the rodent. However, process retraction was not mediated via A2A receptors (Orr et al., 2009) but rather by joint activation of P2Y1 and P2Y13 receptors.

Received Jan. 25, 2019; revised Sept. 27, 2019; accepted Sept. 30, 2019.

Author contributions: G.M., M.M.-B., F.C., G.H., N.R., J.P., L.C., V.N., B.M., S.C., and R.M. designed research; G.M. and M.M.-B. performed research; G.M. and R.M. analyzed data; G.M., M.M.-B., and R.M. wrote the first draft of the paper; G.M. and R.M. edited the paper; G.M. and R.M. wrote the paper; F.C., C.L.D., and E.S. contributed unpublished reagents/analytic tools.

This work was supported by European Research Council Grant 322721 ERC-senior to R.M. and ERAnet Neuron Grant ANR-12-NEUR-0002-03 to R.M. Technical platforms at the ICM are supported by Investissements d'Avenir (ANR-10-IAIHU-06) and NeurATRIS (ANR-11-INBS-0011).

The authors declare no competing financial interests.

Correspondence should be addressed to Giampaolo Milior at giampaolo.milior@college-de-france.fr.

https://doi.org/10.1523/JNEUROSCI.0218-19.2019

Materials and Methods

Tissue from epileptic patients. We compared microglia in tissue from patients diagnosed with two syndromes. Temporal lobe tissue was obtained after operations (Centre Hospitalier Universitaire Pitié-Salpêtrière, Dr. B. Mathon, Dr. S. Clemenceau) on patients diagnosed with pharmacoresistant medial temporal lobe epilepsies (MTLEs) associated with a hippocampal sclerosis (Le Duigou et al., 2018; Morin-Brureau et al., 2018). Tissue was obtained from 8 MTLE patients (age 29–64 years, 4 women, 4 men; left or right temporal lobe sclerosis). Epileptic activities were evident in surface EEG records, and hippocampal sclerosis was confirmed by noninvasive imaging. Cortical tissue was obtained from peritumoral regions (peritumoral cortex [PTC]) in patients diagnosed with cortical brain tumors (Centre Hospitalier Universitaire St. Anne, Dr. J. Pallud; Centre Hospitalier Universitaire Pitié-Salpetrière, Dr. L. Cappelle) (Pallud et al., 2014). Cortical tissue was obtained from 17 patients (age 25–63 years, 5 women, 12 men; 4 diagnosed with astrocytoma, 7 with glioblastoma, 7 with oligodendroglioma; WHO Grades I-IV). Seven of these 17 patients exhibited seizures before surgery. Epileptic activities may have been missed in surface EEG records from the other patients since sites of seizure generation are often restricted and/or deep in the brain. Minimal cauterization during surgery enhanced the quality of tissue slices. Patients all gave a written, informed consent. Protocols were approved by the Comité de protection des personnes, Ile de France 1 (C16-16, 20152482) and followed guidelines of the Comité Consultatif National d'Ethique.

Imaging of microglia in human tissue slices. Tissue handling from the operating room to the laboratory was described by Le Duigou et al. (2018). In brief, tissue was transported in a solution of: 248 mM sucrose, 26 mM $NaHCO_3$, 1 mM KCl, 1 mM $CaCl_2$, 10 mM $MgCl_2$, and 10 mM d-glucose, equilibrated with 95% O_2 and 5% CO_2, at 2°C-10°C. Slices of thickness 300 μm were cut in the same solution in sterile conditions with a vibrating tissue slicer (HM650V, Microm).

We tested two fluorophore-coupled lectins to stain microglia in acute human tissue slices for 2-photon imaging. The B4 isolectin from *Griffonia simplicifolia* (GSA I-B4) labels fixed (Boya et al., 1991) and living microglia (Petersen and Dailey, 2004) as does the tomato lectin from *Lycopersion esculentum* (Acarin et al., 1994; Bordey and Spencer, 2003). Staining was not detected further than ~50 μm from the slice surface, when tomato lectin conjugated to Dy-light 594 (Vector Labs) or B4 isolectin conjugated to AlexaFluor-488 (Thermo Fisher Scientific) was bath-applied. We therefore injected lectins from patch pipettes inserted into middle regions of slices, at > 100 μm from the surface. Lectins were dissolved at 50 μM in a solution of 150 mM NaCl, 2.5 mM KCl, and 10 mM HEPES, pH 7.4 (no added Ca^{2+} or Mg^{2+}) and ejected by gentle positive pressure applied for ~1 min.

Both the tomato lectin and B4 isolectin stained epithelial and endothelial cells of brain blood vessels (Fig. 1*A*). However, only the tomato lectin provided useful staining of human microglia (Schwendele et al., 2012). This staining colocalized with Iba1 immunopositivity (Fig. 1*B*). Fluorescent microglia were resolved at 5–10 min after injection, and strong signals were maintained during observations of duration up to 2–3 h. Possibly the tomato lectin also stains infiltrated peripheral monocytes and macrophages (Ravizza et al., 2008; Varvel et al., 2016). If so, lectin-positive elements, including cells associated with blood vessels, might be described as "tomato lectin-positive cells" (see Discussion). We also used a fluorescent purine (EDA-ADP-ATTO-488, Jena Bioscience) to examine the clearance of purines from slices. It was dissolved in Tris-HCl (1 mM, pH 7.5), and the time course of the loss of fluorescence was compared after ejection into a tissue slice or into bath solution.

2-Photon imaging of microglia. Fluorescent microglia were monitored with an Axio Examiner Z1 microscope (Carl Zeiss) using 2-photon illumination (3i Intelligent Imaging) from a Chameleon Ultra II Ti-sapphire laser (Coherent). Slices of human tissue were placed submerged in a chamber, perfused with a solution of the following: 125 mM NaCl, 26 mM $NaHCO_3$, 3 mM KCl, 2 mM $CaCl_2$, 2 mM $MgCl_2$, and 10 mM d-glucose, equilibrated with 95% O_2 and 5% CO_2 and heated to 30°C–32°C.

The Dy-light 594-coupled tomato lectin was excited at 800 nm and fluorescence detected by a photo-multiplier tube with a 616/69 emission

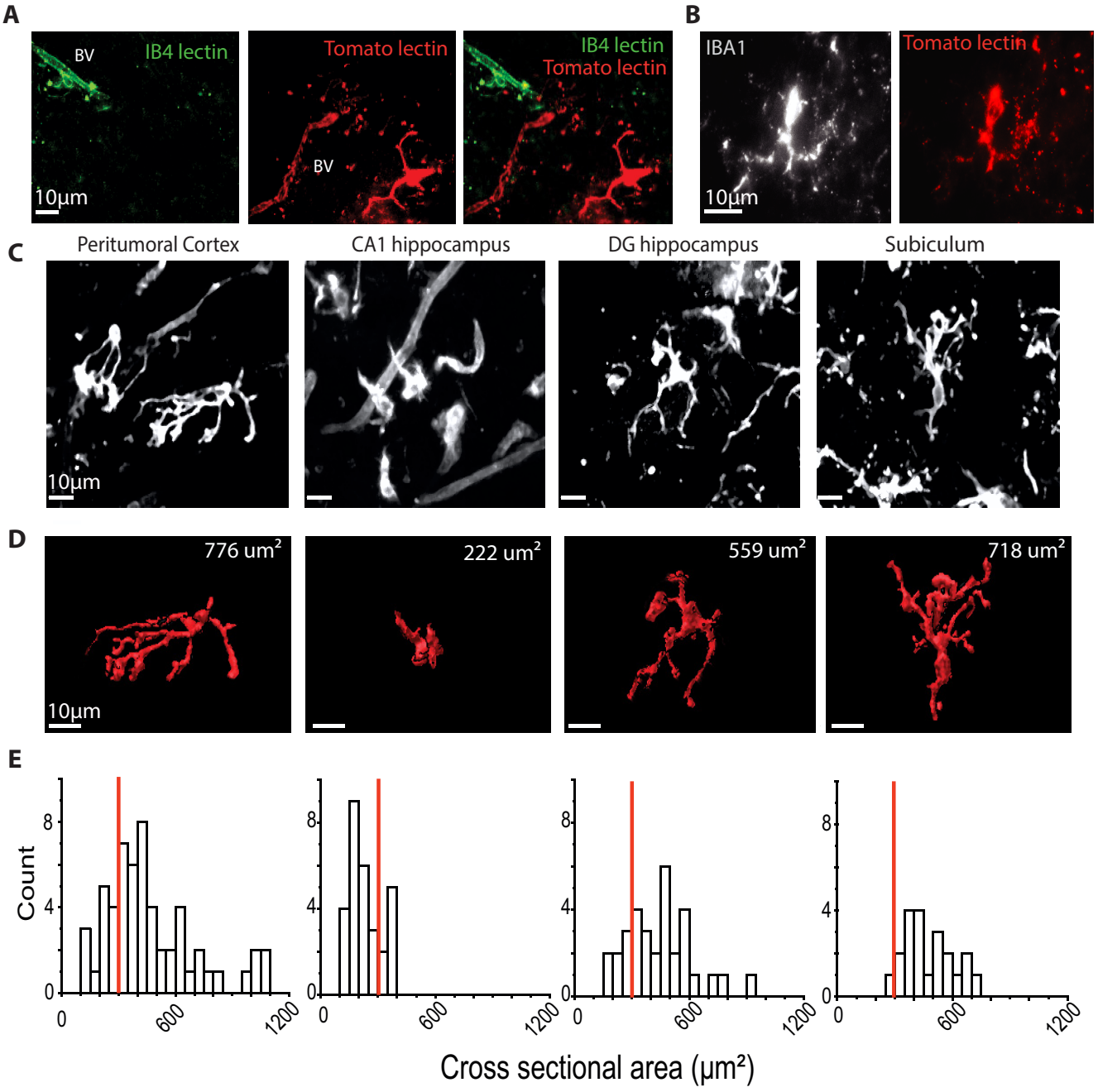

Figure 1. Staining and form of microglia in human PTC and MTLE tissue. ***A***, Staining of PTC with lectin. IB4 (green, left), tomato lectin (red, middle), and both signals (merge). Maximal intensity from *z* stack (total 50 μm, step 1 μm) at 10 min after focal injection of lectins. IB4 lectin stained only endothelial cells of blood vessels (BV). Tomato lectin stained both microglia and endothelial cells. ***B***, Tomato lectin-positive cells (right) were also Iba1$^+$ (left). ***C***, Tomato lectin-labeled microglia from PTC and from the CA1, dentate, and subicular regions of MTLE tissue. Maximal intensity from *z* stacks (50 μm, 1 μm step). ***D***, 3D reconstructions of cells in ***C***. Top right, Cross-sectional area. ***E***, Cross-sectional area distributions for cells of PTC ($n = 34$) and CA1 ($n = 25$), dentate gyrus ($n = 17$), and subiculum ($n = 18$ cells) of MTLE tissue. Red line indicates the threshold of 300 μm^2 used to distinguish amoeboid and ramified cells.

filter and a 580 nm dichroic mirror. IB4 isolectin was excited at 920 nm and fluorescence detected after a 525/40 emission filter and a 580 nm dichroic mirror. Water-immersion objectives of either 20×, NA 1.0 or 40× NA 1.0 (Carl Zeiss) were used. Microglia were monitored after a delay of at least 90 min from slice preparation. Optical sections were collected at *z* intervals 1–2 μm over a depth of 50–70 μm in the middle of slices. Complete *z* stacks could be acquired at intervals of 30–60 s. Images are shown as 2D projections of maximal intensity derived from *z* stacks.

In some experiments, laser stimuli were used to induce tissue damage. Ten to 20 pulses (duration 3 s, wavelength 720 nm, power 400–500 mW) were delivered. Bright-field observations suggested that damage was maximal in a zone of diameter ~10–15 μm at the targeted region.

Image analysis and quantification of microglial shape and motility. Changes in microglial form were measured from sequentially obtained *z* stacks with SlideBook software (3i Intelligent Imaging). We attempted to minimize two possible sources of artefact. First, as microglial processes could overlap with those of lectin-stained blood vessels (Fig. 1*C*), or with those of other microglia during extension, we used minimal volumes of injected lectin to label few microglia. Second, since extending processes could extend beyond previously defined volumes, ROIs were set to allow for process expansion.

The shape of identified, nonoverlapping microglia was represented by a mask created on *z* stack-derived images. Median filtering and deconvolution with a "nearest-neighbor" protocol (SlideBook) reduced noise

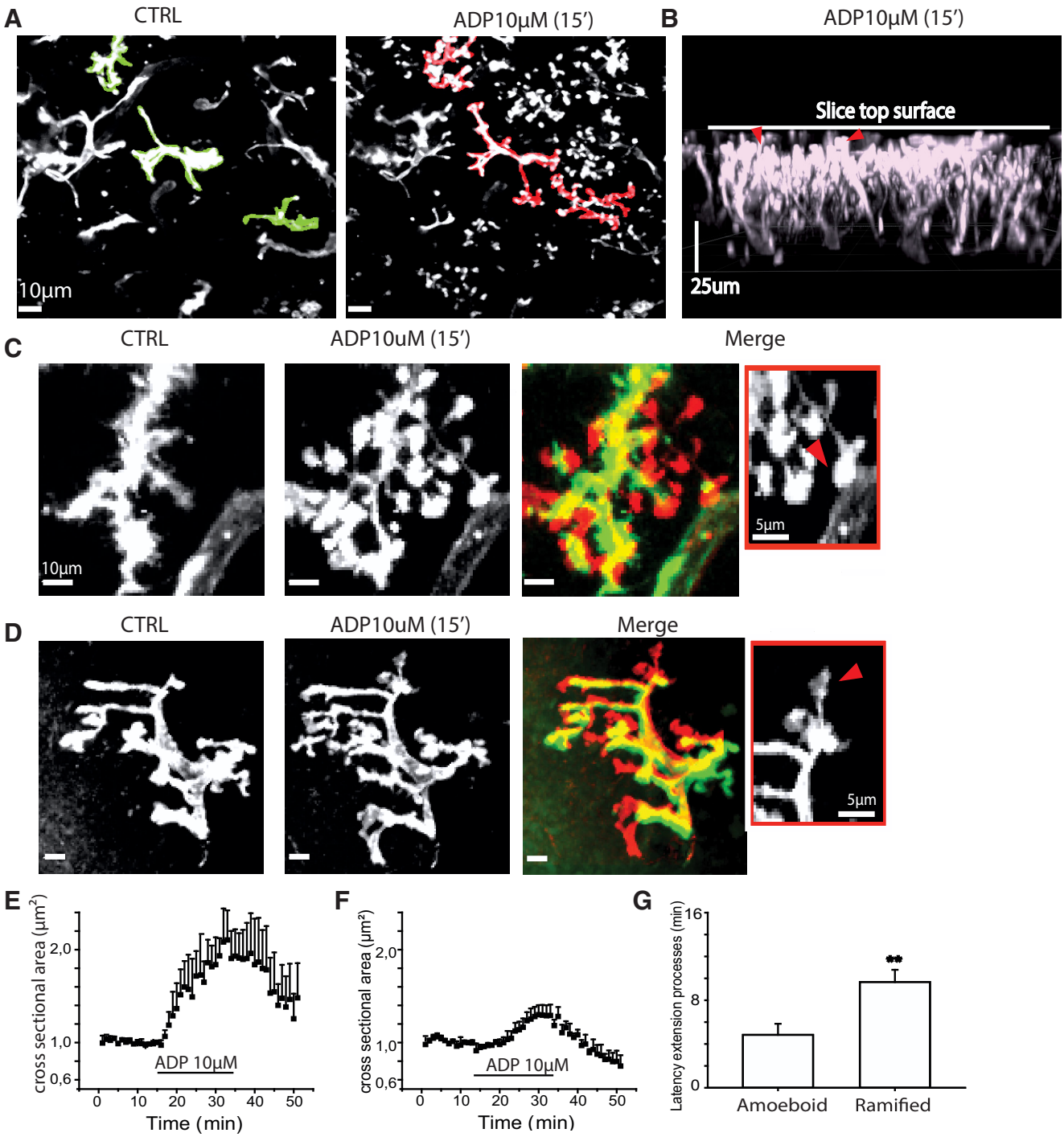

Figure 2. At low doses, ADP induces microglial process extension. ***A***, Tomato lectin stained PTC microglia before (CTRL, left) and after bath application of ADP (10 μM, 15 min, right). Red represents change maximal cross-sectional area (*z* stacks 50 μm, 1 μm). ***B***, Lateral view shows microglial processes extended toward the upper surface of the slice. Red arrows indicate bulbous endings at their tips. ***C***, ADP at low doses induces process emergence and extension from an amoeboid cell. Images are control (CRTL, left) and ADP (10 μM, 15 min, middle). Right, Merge image represents color-coded differences between CTRL and ADP images. Red represents new signal; green represents lost signal; yellow represents maintained signal (*z* stack 20 μm, 1 μm). Right, Inset, Bulbous endings (red arrow) at the tips of processes. ***D***, ADP induces process extension of a ramified microglia. Control (CRTL, left), ADP (10 μM, 15 min middle), and color-coded differences between them (merge image, right). Red represents new signal; green represents lost signal; yellow represents maintained signal (*z* stack 20 μm, 1 μm, scale bar 10 μm). Inset, Bulbous endings (red arrow) at process tips. ***E***, Time course of changes in mean cross-sectional area induced by 10 μM ADP in 7 amoeboid microglia. ***F***, Time course of changes in mean cross-sectional area induced by 10 μM ADP in 7 ramified microglia. ***G***, Mean and SE of the latency to 20% increase in cross-sectional area induced by ADP for amoeboid ($n = 7$) and ramified microglia ($n = 7$). Process extension by ramified cells occurred at a significantly longer latency (*t* test, $p = 0.009$**). Movie 1 shows process extension of an amoeboid cell induced by low-dose ADP.

and improved the resolution of fluorescent cells. Masks were created using a "segment mask" tool, defined by Otsu thresholding (SlideBook). The "refine object" tool was used for manual correction of threshold or shape, if needed. Finally, the "mask statistics" tool was used to follow the time course of changes in microglial cross-sectional area (μm^2) derived from maximal 2D projections from *z* stacks. Cell volume was derived from complete 3D reconstructions of unstimulated single cells or maximally extended or retracted states after purinergic stimuli.

Ruffling, continuous extrusion and retraction of microglial surface membrane (Bianco et al., 2005) was quantified by subtracting sequential 2D maximal projections at defined time intervals. Color coding of membrane lost or gained between sequential time points was used to illustrate process extension and retraction.

Purinergic stimulation of microglia: agonists and antagonists. We examined microglial mobility and motility responses to bath application of purinergic agonists and antagonists. Slice preparation might alter the form and motility of human microglia. To reduce such possible artifacts, the effects of purines were not tested until at least 2 h after slices were prepared. Response latencies were measured from the time of switching to the purine containing solution. Latencies include a delay of ~60 s for new solution to reach sites within a slice. Effects of purines on microglial processes were measured at a latency of 20 min after switching between solutions, unless noted otherwise.

Initial data were obtained with ADP (10 μM to 2 mM) and ATP (10 μM to 2 mM). Since purines are hydrolyzed by intrinsic tissue ectonucleotidases (from ATP to ADP to adenosine) (Yegutkin, 2014), we also examined responses to a nonhydrolyzable ADP analog, 2MeSADP (2-methylthioadenosine diphosphate trisodium; 0.001–2 μM), a nonhydrolyzable ATP analog, 2MeSATP (2-methylthioadenosine triphosphate tetra sodium, 0.1–100 μM), and the stable adenosine analog, 2-chloroadenosine (10–100 μM). 2MeSADP is an agonist at P2Y1, P2Y12, and P2Y13 receptors. 2MeSATP is an agonist at P2Y1, P2Y6, and P2Y13 as well as P2X receptors. 2-Chloro-adenosine is an agonist at A1, A2A, A2B, and receptors (Abbracchio et al., 2019).

We examined effects on these responses of specific antagonists at distinct purinergic and adrenergic receptors. As P2Y12 receptor antagonists, we used PSB0739 (Tocris Bioscience, 0.1–5 μM) (Baqi et al., 2009) and Ticagrelor (Cayman, 1–10 μM) (Cattaneo, 2010). MRS2279 (Tocris Bioscience, 1–10 μM) (Shinozaki et al., 2014) and MRS2500 (Tocris Bioscience, 1–10 μM) (Quintas et al., 2018) were used as antagonists at P2Y1 receptors. MRS2211 (Tocris Bioscience, 5–30 μM) (Kim et al., 2005) was used as a P2Y13 antagonist. As A2A receptor antagonists, we used Preladenant (Sigma Millipore, 5 μM) (Neustadt et al., 2009) and SCH-58261 (5 μM) (Orr et al., 2009). MRS2578 (Tocris Bioscience, 10 μM) was used as P2Y6 antagonist (Riegel et al., 2011).

Immunostaining and imaging. Tissue slices (200–300 μm) were fixed for immunostaining by immersion for 2 min in 4% phosphate-buffered PFA heated to 80°C. High temperatures enhance diffusion and accelerate fixation in slices (Dissing-Olesen and MacVicar, 2015). Immunostaining was performed on fixed slices (200–300 μm) washed in 0.1 M PBS containing 20% DMSO and 2% Triton ×100. Slices were blocked in 3% BSA (24 h) and then incubated with a primary antibody together with 1% BSA for 7 d at 4°C.

We used primary antibodies directed against the following: Iba1 (Abcam, ab5076; 1/500), P2Y12 (Novus, NBP2–33870; 1/200), A2AR (Santa Cruz Biotechnology, sc-32261; 1/100), P2Y1 (Abcam, ab168918; 1/200), and P2Y13 (LSBio, LS-A1622; 1/200). Slices were incubated for 6 d with secondary antibodies: IgG conjugated with Alexa-488, -555, or -647. These long exposures to primary and secondary antibodies should enhance penetration throughout fixed slices (Dissing-Olesen and MacVicar, 2015). After exposure slices were mounted in Fluorosave (Merck) on microscope slides with a cover glass elevated by 300 μm (Fisher Scientific).

Structured images were made with an Olympus IX81 fluorescent microscope equipped with filters for 4 emitted light wavelengths and visualized with Retiga EXI camera (Qimaging). Stacks of 10–30 images at z interval 0.5–1.0 μm were acquired with oil-immersion objectives (40×, NA 1.3 or 60×, NA 0.9).

Experimental design and statistical analysis. Data are mean ± SEM. Statistical analysis was done and graphs produced using Origin Pro 2016 software. The significance of differences between groups was assessed with the unpaired, two-sided Student's t test, with $p \leq 0.05$ considered significant. Differences within subjects were assessed with the paired, two-sided Student's t test with $p \leq 0.05$ considered significant.

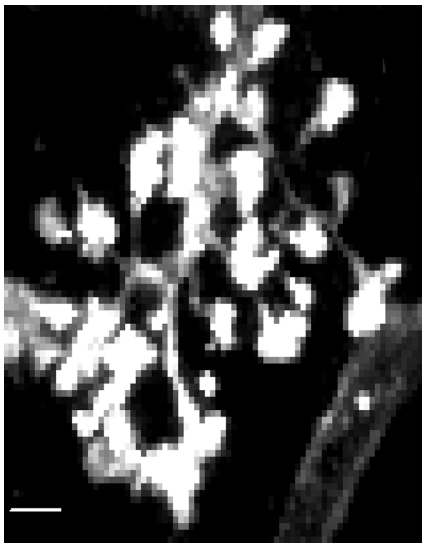

Movie 1. Process extension of an initially amoeboid, tomato lectin-labeled microglia from PTC induced by 10 μM ADP applied at time counter = 10.00 min. Scale bar 5 μm, bottom left. Frame rate 3/s.

Results

Lectin-labeled microglia in tissue from patients with MTLE and PTC

Tomato lectin-labeled microglia in human MTLE and PTC tissue were heterogeneous in form, with features that were consistent between tissues. Figure 1*C* shows examples of cells from PTC tissue and from the dentate, CA1 region, and subiculum of MTLE-HS tissue. Three-dimensional reconstructions of these cells are shown in Figure 1*D*, and distributions of cross-sectional area for cells from each region (n = 21–58) are plotted in Figure 1*E*.

Cells of the subiculum typically possessed multiple ramified processes similar to surveilling microglia of the rodent (Hanisch and Kettenmann, 2007). In contrast, microglia from the CA1 region where few neurons survived (Blümcke et al., 2013) were often smaller with fewer, shorter processes or no processes. Rodent cells with these shapes have been termed "activated" and "reactive" microglia (Streit et al., 1988; Davis et al., 1994). Initial work on human epileptic tissue identified many "reactive" microglia (Beach et al., 1995). Microglia of PTC exhibited a similar range of shapes. The density of tomato lectin-positive cells with few processes was higher near the tumor (Buckingham and Robel, 2013). The cross-sectional area of cells with no processes, in MTLE and PTC tissue, was typically 70–180 μm^2. We will not differentiate between "reactive" and "activated" microglia but rather class cells with cross-sectional areas <300 μm^2 (Fig. 1*E*, red lines) and with two or less processes as amoeboid cells, and those with areas >300 μm^2 and more than two processes as ramified (Buckingham and Robel, 2013; Morin-Brureau et al., 2018).

Responses of microglia to purinergic stimulation

We monitored fluorescent microglia in tissue slices from patients diagnosed with MTLE and in peritumoral slices from patients with cortical gliomas (PTC). In our previous work, ~95% of MTLE tissues generate spontaneous interictal-like epileptic activ-

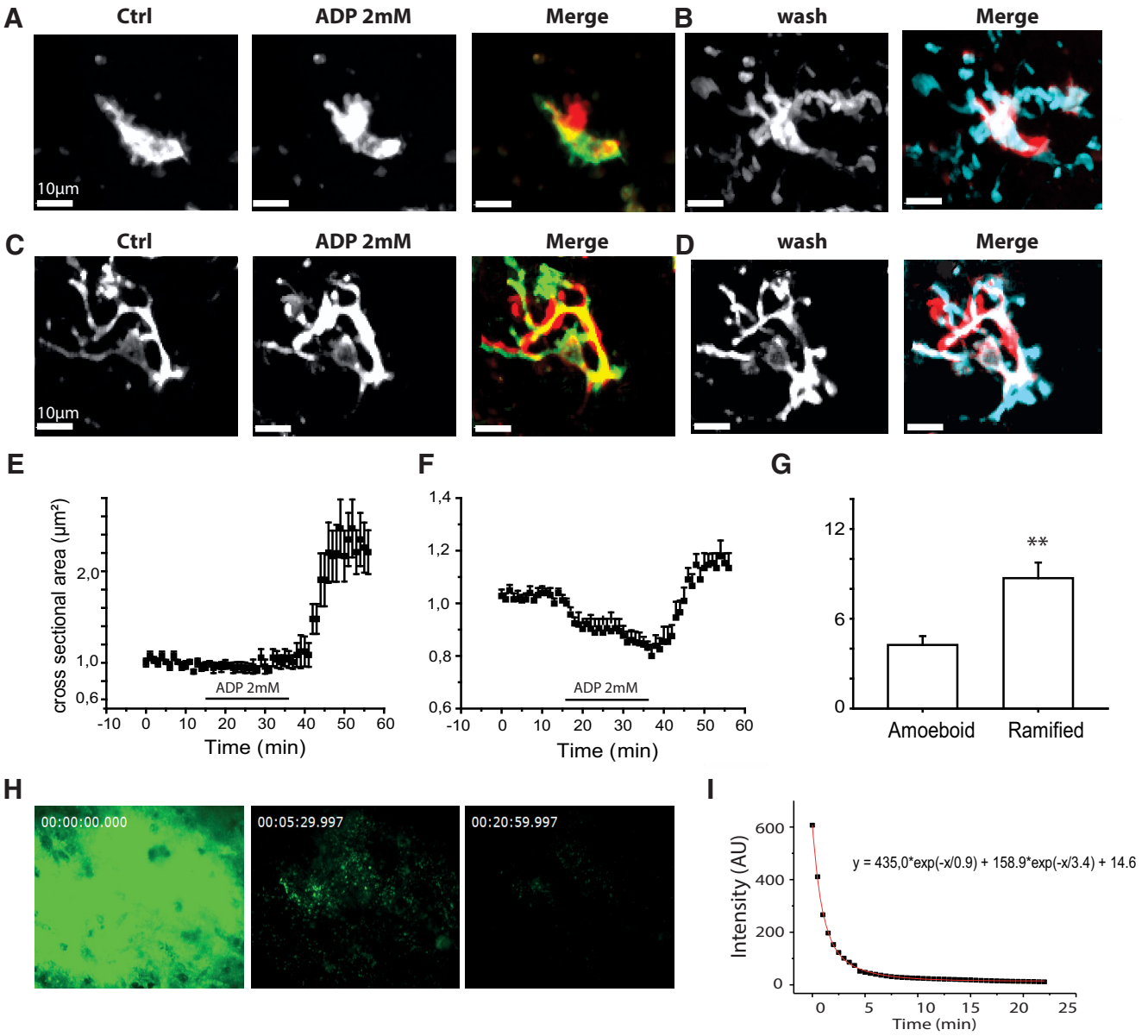

Figure 3. High doses of ADP induce microglial process retraction and membrane ruffling. ***A***, ADP induces membrane ruffling of amoeboid microglia. Control (left), ADP (2 mM, 20 min, middle). Right, Merge image represents color-coded differences. Red represents new fluorescent signal; green represents lost signal; yellow represents maintained signal. ***B***, Transition from 2 mM ADP back to control for the same cell (wash, left) induces process extension. Right, Merge image represents differences from ADP. Blue represents new signal; red represents lost signal. ***C***, ADP induces process retraction and membrane ruffling of ramified microglia. Control (left), ADP (2 mM, 20 min, middle). Right, Merge represents differences. Blue represents new signal; green represents lost signal; yellow represents maintained signal. ***D***, Transition from ADP back to control for the cell in ***C*** induces process extension (wash, left). Right, Merge image represents color-coded differences. Blue represents new signal; red represents lost signal. ***A–D***, Maximal projections from *z* stacks (50 μm, 2 μm step). ***E***, Time course of changes in mean cross-sectional area in 7 initially amoeboid cells. Little change occurs during application of 2 mM ADP application. Processes extend when ADP is removed. ***F***, Time course of the reduction in mean cross-sectional area induced by 2 mM ADP in 9 ramified microglia. Processes extend when ADP is removed. ***G***, Different latencies to process extension (increase of 20% for cross-sectional area) during the transition from 2 mM ADP back to control ACSF. The latency is significantly longer for ramified microglia (*t* test, $p = 0.004^{**}$). Movie 2 shows membrane ruffling of amoeboid microglia induced by 2 mM ADP. Movie 3 shows process retraction of a ramified microglia induced by 2 mM ADP. ***H***, Fluorescence at 0, 5, and 20 min after focal ejection of the fluorescent purine EDA-ADP-ATTO-488 at 1 mM from a patch pipette into middle regions of a 300-μm-thick PTC slice. ***I***, The decay followed a double exponential time course with fastest decay in the first 3–5 min. The fit was $y = 435.0 \times \exp(-x/0.9) + 158.9 \times \exp(-x/3.4) + 14.6$, where *y* is fluorescence and *x* is time. Fluorescence was maintained longer than 20 min after ejection into the slice but decayed in 2–3 s after ejection into the bath.

ity (Huberfeld et al., 2011) while such activity is recorded from ~70% of PTC tissue slices (Pallud et al., 2014). Amoeboid microglia of MTLE or PTC tissue moved little in control conditions. Processes of ramified microglia of MTLE or PTC extended and retracted constantly while their somata moved little.

Different doses of ADP or ATP, applied by bath, induced opposing effects on microglial motility. Low doses (1–10 μM for 15–30 min) induced microglial process extension (Fig. 2*A*). Processes typically extended toward the surface of the slice and terminated in bulb-like endings (Fig. 2*B*). In amoeboid cells, application of 10 μM ADP (Fig. 2*C*; Movie 1) induced a significant increase of 80 ± 18% in cross-sectional area ($p = 0.004$; $t = -4.37$; $n = 7$, 3 MTLE and 4 PTC cells; Fig. 2*E*), transforming them into ramified cells. New processes appeared at a latency of 2–8 min (mean 5.0 ± 1.2 min; Fig. 2*G*). The mean volume of amoeboid cells increased significantly from 296.5 ± 34.5 μm^3 to 555.8 ± 106.9 μm^3 at full extension (1 MTLE and 4 PTC cells; $p = 0.03$; $t = -3.23$).

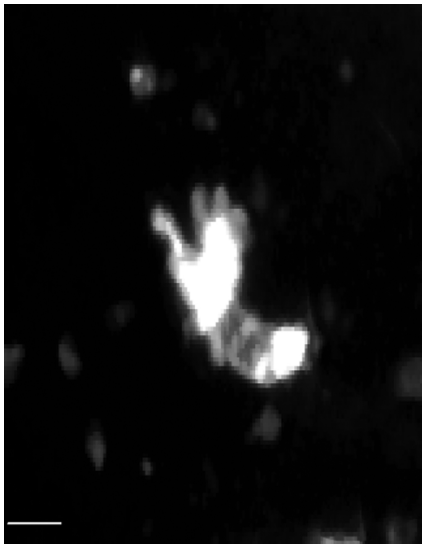

Movie 2. Membrane ruffling of an initially amoeboid cell from the sclerotic CA1 region of MTLE tissue on application of 2 mM ADP, at time counter = 5.40 min. Followed by process extension when ADP was removed, at time counter = 45.25 min. Scale bar 10 μm, bottom left. Frame rate 3/s.

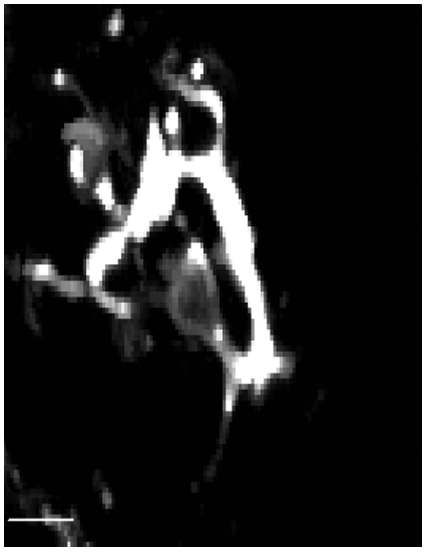

Movie 3. Process retraction and membrane ruffling of an initially ramified cell from PTC induced by application of 2 mM ADP at time counter = 7.13 min. Followed by vigorous process extension when ADP was removed, at time counter = 49.04 min. Scale bar 10 μm, bottom left. Frame rate 3/s.

In ramified cells, 10 μM ADP (Fig. 2*D*) also significantly increased mean cross-sectional area by 39 ± 9% ($p = 0.01$; $t = -3.42$; 3 MTLE and 4 PTC cells; Fig. 2*F*). Process extension was initiated at a latency of 6–12 min (mean 9.4 ± 1.4 min; $n = 3$ MTLE and 4 PTC microglia). The latency to a 20% increase in cross-sectional area was consistently greater for ramified than for amoeboid microglia ($p = 0.009$; $t = 3.2$; Fig. 2*G*). The mean volume of ramified cells increased significantly from a control value of 709.2 ± 74.3 μm^3 to 900.2 ± 30.4 μm^3 at full extension ($p = 0.03$; $t = -3.17$; $n = 5$, 1 MTLE and 4 PTC cells; data not shown).

Thus, low doses of ADP induced process extension for both initially amoeboid and ramified microglia. Percentage increases in cross-sectional area and absolute increases in microglial volume were larger for amoeboid cells. Similar responses were induced by 10 μM ATP ($n = 5$, 2 MTLE and 3 PTC cells not shown).

Higher doses of ADP or ATP (1–2 mM for 30 min) triggered distinct changes in microglial motility. Amoeboid cells exhibited ruffling (Fig. 3*A*; Movie 2), continuous advances, and retractions often of perisomatic membrane (Bianco et al., 2005), but 2 mM ADP induced only minor changes (mean 7 ± 12%) in their cross-sectional area ($p = 0.6$; $t = -0.56$; 3 MTLE cells, 4 PTC cells; Fig. 3*E*). Processes of ramified cells ceased surveillance movements in response to 2 mM ADP. They then retracted with a latency of 5–10 min (mean 3.4 ± 1.1 min; Fig. 3*C*; Movie 3). The cross-sectional area of ramified cells was reduced by 18 ± 2% ($p < 0.001$; $t = 6.04$; 5 MTLE cells and 4 PTC cells; Fig. 3*F*). The volume of initially ramified cells was reduced significantly from 721.6 ± 96.5 μm^3 to 573.7 ± 92.2 μm^3 ($p < 0.001$, $t = 6.52$; 5 MTLE and 2 PTC cells). Processes of initially ramified microglia did not retract so far as to convert them into amoeboid cells. Membrane ruffling occurred in ramified cells when retraction was complete. Cells tested with high-dose ADP were not the same as those tested with low-dose ADP.

Unexpectedly, process of both ramified and amoeboid microglia extended on switching from 2 mM ADP back to control ACSF (Fig. 3*B*,*D*). This rebound extension consisted of a significant increase (120 ± 23%) in cross-sectional area of amoeboid cells ($p < 0.001$; $t = -6.40$, 3 MTLE cells, 4 PTC cells; Fig. 3*E*; Movie 2). This extension is comparable to that induced by 1–10 μM ADP. Rebound process extension occurred for all ramified microglia on switching to control ACSF (5 MTLE cells and 4 PTC cells; Fig. 3*F*; Movie 3). The mean increase in cross-sectional area after ADP withdrawal was 31 ± 5% ($p < 0.001$; $t = -5.44$). As for process extensions induced by low purine doses, the latency to rebound extension was consistently greater for ramified than for amoeboid microglia ($p = 0.002$; $t = 3.86$; Fig. 3*G*).

A similar processes extension was induced on switching from 2 mM ADP to 10–50 μM ADP ($n = 4$ cells not shown). This tends to suggest that the extension may have resulted from exposure to low levels of ADP during slow clearance from slices. We examined this possibility by comparing the decay of signals from a fluorescent purine (EDA-ADP-ATTO-488, 1 mM) ejected from a patch pipette in the bath or in middle regions of a tissue slice (Fig. 3*H*). Signals decayed in 2–3 s after ejection into the bath. In contrast, they decayed more slowly with a double exponential time course when ejection was made into the slice (Fig. 3*I*). Fluorescence levels at 20 min remained at 1.5%–2% of peak values.

Intermediate purine doses (100–500 μM ADP, 15–30 min) could initiate either process retraction or extension in different neighboring cells. We analyzed relations between ADP dose (1 μM to 2 mM) and percentage change in cross-sectional area for 15 amoeboid and 16 ramified cells (data not shown). Maximal mean increases in cross-sectional area (63 ± 15%; $p = 0.002$, $t = -4.1$) occurred in response to 10 μM ADP. Maximal reductions (−16 ± 5%; $p = 0.009$; $t = 3.10$) were induced by 2 mM ADP. Process extension when purinergic stimulation ceased was most strong for the highest dose, 2 mM ADP. This switch between two distinct responses, process extension for low doses and retraction for high purine doses, was comparable for both amoeboid and ramified microglia.

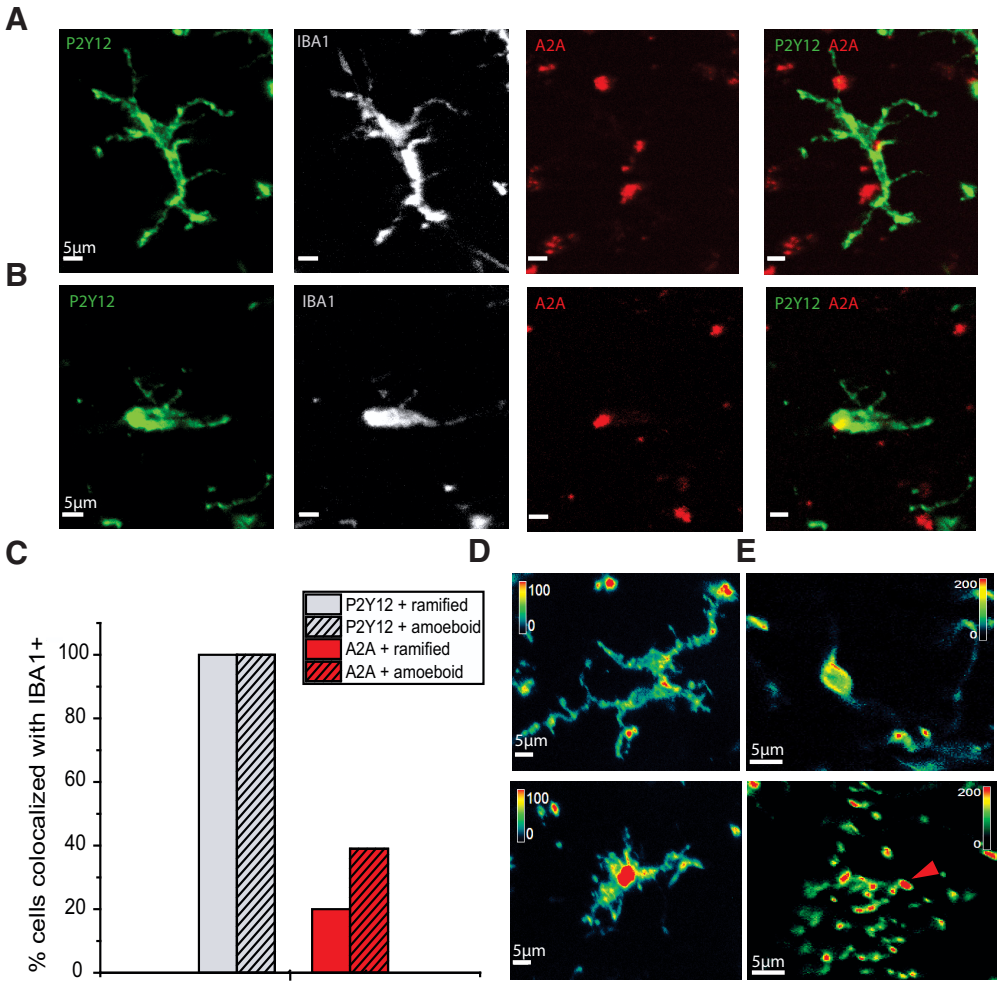

Figure 4. Expression of P2Y12 and A2A receptors by human microglia. ***A***, Immunostaining against P2Y12 and A2A receptors in an IBA1$^+$, ramified PTC microglia. ***B***, P2Y12 and A2A receptor immunostaining for an amoeboid IBA1$^+$ cell from MTLE tissue. ***A***, ***B***, From left, P2Y12 immunostaining (green), IBA1 (white), A2A (red), and merged P2Y12 and A2A staining. ***C***, Proportion of ramified (clear; $n = 33$) and amoeboid (hatched; $n = 25$) microglia immunopositive for P2Y12 (gray) and A2A receptors (red). ***D***, Color-coded staining intensity (green represents low; red represents high) shows that P2Y12 staining was highest toward the tips of processes of a ramified microglia (above) in the resting state. Intensity was highest in a somatic region of a nonstimulated amoeboid cell (below). ***E***, Color-coded intensity (green represents low; red represents high) for P2Y12 immunopositivity for initially amoeboid microglia fixed at full extension induced by 10 μM ADP. Staining intensity was low in perisomatic regions (top) and highest at bulbous endings of processes (bottom).

Furthermore, microglia of MTLE and PTC tissue tended to behave in the same way. Mean process extension induced by 10 μM ADP was 51 ± 12% in 4 ramified PTC cells and 42 ± 3% in 3 ramified MTLE cells ($p = 0.48$; $t = 0.75$; not significantly different; data not shown). Process extension induced by low-dose ADP was 92 ± 27% for 4 amoeboid PTC cells and 67 ± 14% for 3 amoeboid cells from MTLE tissue ($p = 0.61$; $t = 0.53$; not significantly different; data not shown). Process retraction induced by 2 mM ADP was 18 ± 4% for 4 ramified PTC cells and 13 ± 3% for 5 ramified MTLE cells ($p = 0.72$; $t = -0,35$; not significantly different; data not shown). With these similarities, cells from PTC and MTLE tissues will be considered together in the following data.

Evidence for receptor expression

These opposing microglial motilities may depend on distinct receptors. In rodents, activation of the P2Y12 receptor initiates microglial process extension (Haynes et al., 2006). Reciprocally, purinergic stimuli induce process retraction by microglia in an inflammatory context (Gyoneva et al., 2014) via upregulated A2A receptors (Orr et al., 2009).

Tissue from epilepsy patients is in an inflammatory state, and some microglia have an amoeboid shape (Beach et al., 1995; Buckingham and Robel, 2013; Morin-Brureau et al., 2018). We therefore asked whether amoeboid or ramified cells of MTLE and PTC tissue express P2Y12 and A2A receptors by immunostaining with specific antibodies (Fig. 4). All Iba1$^+$ cells in both types of tissue (Fig. 4*A*,*B*) were immunopositive to an antibody against P2Y12 receptors (Moore et al., 2015; Mildner et al., 2017). P2Y12 staining was detected, typically throughout microglia membrane and cytoplasm, for all amoeboid cells ($n = 25$) and all ramified microglia ($n = 33$) from MTLE-HS or PTC tissue (Fig. 4*C*).

In contrast, fewer Iba1$^+$ microglia were immunopositive for A2A receptors, and cellular staining was less uniform (Fig. 4*A*,*B*). A2A immunostaining was also evident outside microglia, suggesting that the receptor was expressed by other cell types, unlike P2Y12 staining. A2A and Iba1$^+$ immunostaining was both detected in 13 of 25 amoeboid cells and 7 of 33 ramified microglia from a MTLE-HS or PTC tissue (Fig. 4*C*).

We also asked whether membrane distributions of these receptors altered during process extension or retraction induced by

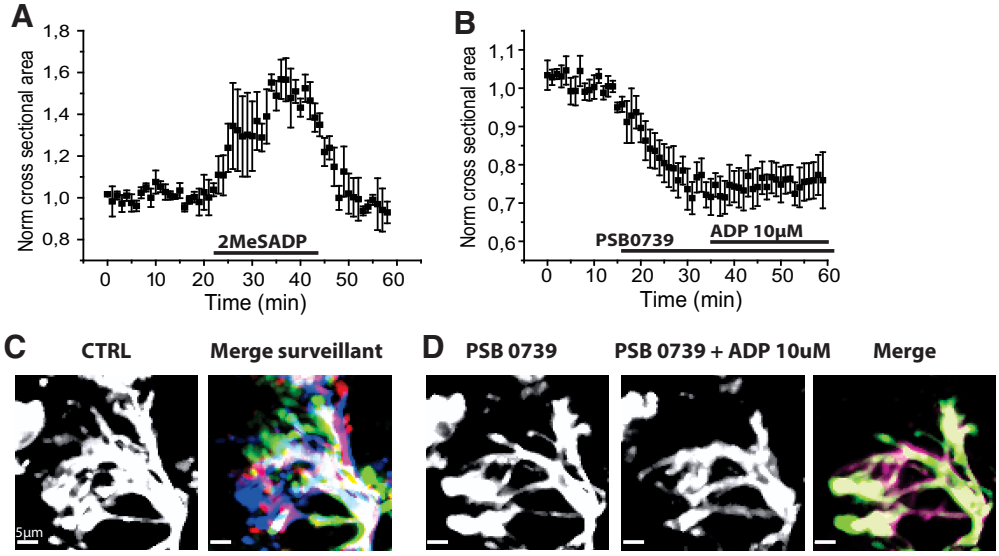

Figure 5. P2Y12 receptors and microglial motilities. ***A***, The nonhydrolyzable ADP analog 2MeSADP (1 nM) increased mean microglial cross-sectional area ($n = 4$ PTC cells). ***B***, The P2Y12 receptor antagonist PSB0739 (1 μM) reduced the mean cross-sectional area of ramified microglia (3 PTC and 2 MTLE microglia). It prevented the process extension induced by 10 μM ADP. ***C***, PSB0739 suppressed surveillance motility of processes of ramified microglia. Right, Control. Left, Process positions at 5 min intervals during control period shown by colors (green, red, yellow, dark blue, light blue). ***D***, Right, After PSB0739. Middle, Processes in the presence of PSB0739 (1 μM) and ADP (10 μM). Left, Process positions at 5 min intervals (colors as in ***C***). Movie 4 shows that PSB0739 suppresses surveillance motility and blocks ADP-induced process extension.

purinergic agonists. For microglia fixed in the resting state, P2Y12 receptor immunostaining was most intense at junctions between processes or toward process extremities (Fig. 4*D*). When slices were fixed after process extension induced by low doses of ADP, the highest intensities of immunostaining were detected at the bulbous tips of microglial processes (Fig. 4*E*).

Purine receptor subtype underlying process extension

We sought pharmacological evidence that the activation of distinct purinergic receptors underlies extension or retraction of microglial processes. Receptor identification is not simple because intrinsic tissue ecto-enzymes can hydrolyze ATP to ADP and ADP to adenosine (Dale, 1998; Yegutkin, 2014). We therefore used a nonhydrolyzable ADP analog, 2MeSADP (1 nM), which activates P2Y1, P2Y12, and P2Y13 receptors (Abbracchio et al., 2019). Figure 5*A* shows 2MeSADP induced process extension of amoeboid microglia. 2MeSADP application significantly increased cross-sectional area by 49 ± 9% ($p = 0.01$; $t = -5.33$, $n = 2$ MTLE cells, 2 PTC cells) but did not provoke membrane ruffling ($n = 2$ MTLE cells, 2 PTC cells).

Figure 5*B–D* shows the effects of the specific P2Y12 antagonist PSB0739 (Baqi et al., 2009). At 0.1–1 μM, PSB0739 application led to a rapid cessation of surveilling movements (Fig. 5*C*; Movie 4) and the retraction of processes of ramified microglia (Fig. 5*D*; Movie 4). Cross-sectional area was significantly reduced by 25 ± 3% after PSB0739 application ($p = 0.002$; $t = 7.47$; $n = 3$ PTC cells, $n = 2$ MTLE cells; Figure 5*B*). These data suggest that tonically activated P2Y12 receptors contribute to the control of process length and surveillance movements (Matyash et al., 2017). To confirm this point, we tested Ticagrelor, another P2Y12 receptor antagonist. Ticagrelor (1–5 μM; data not shown) also suppressed surveillance movements of ramified cells. Cross-sectional area was significantly reduced by 27 ± 5% by Ticagrelor ($p = 0.01$; $t = 5.00$; $n = 4$ ramified microglia, all MTLE). Thus, P2Y12 receptor antagonists suppress surveillance movements and reduce microglial process cross-sectional area to an extent comparable to 2 mM ADP.

Movie 4. Process retraction and cessation of surveillance motility of a ramified microglia of PTC induced by PSB0739 (1 μM) applied at time counter = 11.00 min. ADP at 10 μM applied in the presence of PSB0739 at time counter = 25.00 min does not induce process extension. Scale bar 5 μm, bottom left. Frame rate 3/s.

We next asked whether PSB0739 (1 μM) or Ticagrelor (5 μM) affected process extension induced by 10 μM ADP (Fig. 5*B*; Movie 4). In 5 amoeboid microglia, increases in cross-sectional area were suppressed in the presence of PSB0739 (data not shown). Similarly, 10 μM ADP no longer induced extension of processes of ramified cells in the presence of PSB0739. The change in cross-sectional area for 7 cells was 5 ± 3% ($p = 0.13$; $t = -1.72$; Fig. 5*B*; $n = 7$; 5 PTC, 2 MTLE; Fig. 5*B*). Process extension was also suppressed by Ticagrelor (5 μM; $n = 3$ cells; data not shown), and extension observed on withdrawal of 2 mM ADP was also suppressed by PSB0739 ($n = 5$ cells; data not shown).

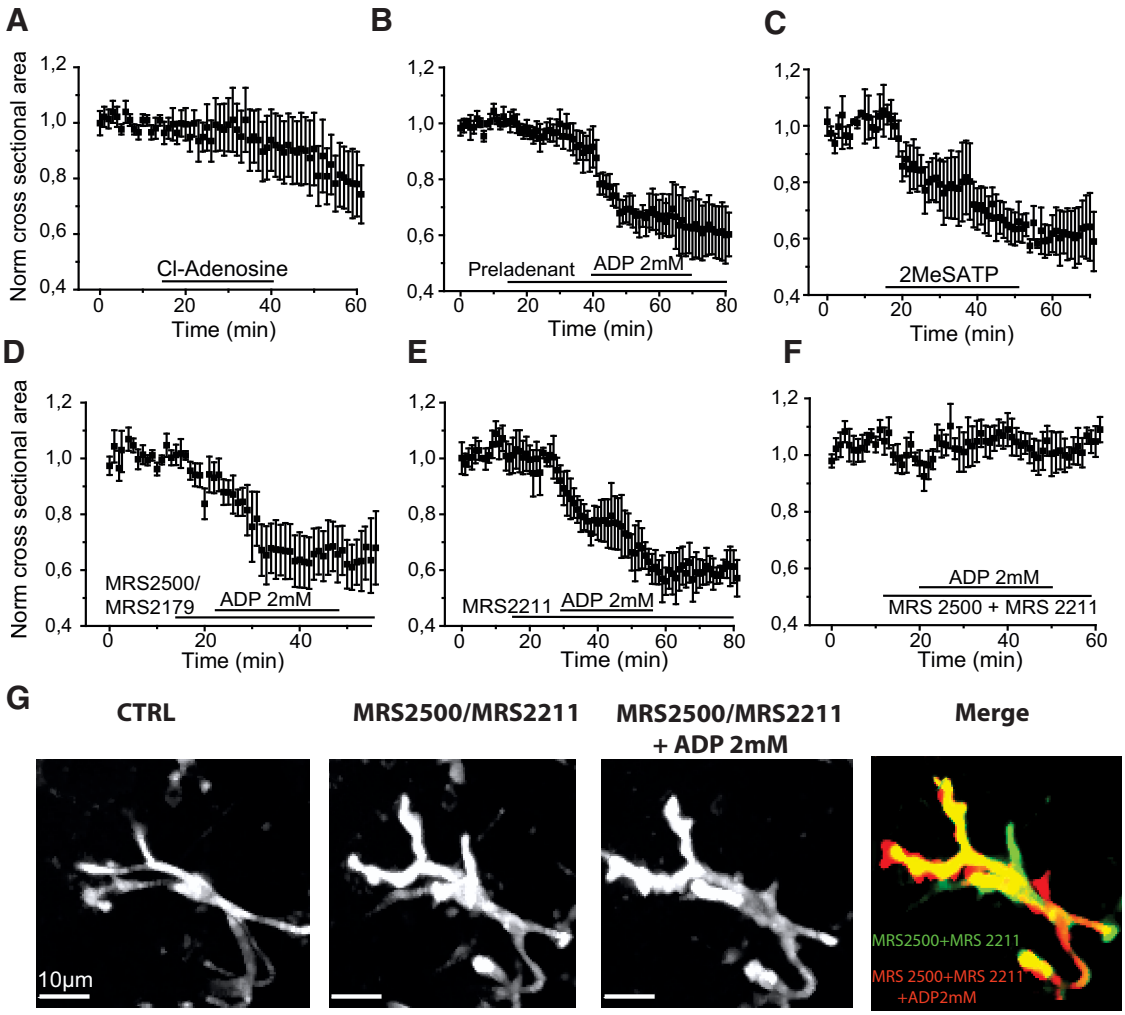

Figure 6. Receptors involved in microglial process retraction. ***A***, The stable adenosine analog 2-chloro-adenosine (100 μM) induced a small reduction in mean microglial cross-sectional area (4 MTLE and 2 PTC ramified cells). ***B***, The A2A receptor antagonist Preladenant (5 μM) did not suppress process retraction induced by 2 mM ADP (mean, normalized data from $n = 4$ ramified PTC cells). ***C***, The nonhydrolyzable ATP analog 2MeSATP (100 μM) reduced the mean cross-sectional area of 3 ramified microglia of MTLE tissue. ***D***, P2Y1 receptor antagonists MRS2500 or MRS2179 (10 μM) did not prevent the reduction of microglial cross-sectional area induced by 2 mM ADP in ramified microglia (4 MTLE, 2 PTC cells). ***E***, The P2Y13 antagonist MRS2211 (30 μM) did not suppress process retraction induced by 2 mM ADP in 4 ramified PTC microglia. ***F***, Coapplication of MRS2500 (10 μM) and MRS2211 (30 μM) suppressed retraction induced by 2 mM ADP (5 ramified cells: 2 MTLE, 3 PTC cells). ***G***, Response of an initially ramified microglia (PTC) to 2 mM ADP in the presence of MRS2500 (10 μM) and MRS2211 (30 μM). From left, CTRL, basal state, in the presence of both antagonists, and then 2 mM ADP. Merge image represents the difference between cell shape in the presence of both antagonists and then after applying ADP. Red represents new fluorescent signal; green represents lost signal; yellow represents maintained signal. Movie 5 shows that the coapplication of P2Y1 and P2Y13 receptor antagonists suppresses process retraction.

In summary, human microglia of amoeboid or ramified form were all P2Y12$^+$ (Fig. 5). Antagonists of these receptors blocked process extension and also suppressed surveillance movements, revealing a tonic action of P2Y12 receptor activation.

Purine receptor subtype initiating microglial ruffling and process retraction

We asked whether adenosine receptor activation was involved in microglial process retraction or membrane ruffling induced by higher doses of purines. The stable broad-spectrum analog 2-chloro-adenosine (100 μM) was used to activate adenosine receptors. It induced a small reduction (8 ± 10%) in cross-sectional area of ramified microglia ($p = 0.46$; $t = 0.79$; 2 PTC, 4 MTLE cells; Fig. 6*A*) but did not induce membrane ruffling of amoeboid microglia (2 PTC, 4 MTLE cells).

Next, we tested the effects of specific A2A receptor antagonists Preladenant and SCH58261 on the process retraction induced by 2 mM ADP. In 5 μM Preladenant, ADP application significantly reduced microglial cross-sectional area by 36 ± 3% ($p = 0.001$; $t = 10.33$ $n = 4$ PTC cells; Fig. 6*B*). Similarly, SCH58261 (5 μM) did not prevent process retraction induced by ADP. 2 mM ADP reduced cross-sectional area by 47 ± 9% in the presence of SCH58216 ($p = 0.03$; $t = 5.13$; 3 PTC microglia). In summary, not all microglia, including amoeboid cells, express A2A receptors (Fig. 5). Antagonists of these receptors did not suppress process retraction induced by strong purinergic stimuli.

If adenosine receptors are not involved in process retraction, might P2Y receptors be responsible? We turned to another broad-spectrum agonist, the nonhydrolyzable ATP analog, 2MeSATP, which activates P2Y1, P2Y13, and P2Y6, but not P2Y12 receptors (Abbracchio et al., 2019). 2MeSATP (100 μM) reduced microglial cross-sectional area significantly by 31 ± 6% ($p = 0.04$; $t = 4.73$; 3 ramified PTC microglia; Fig. 6*C*). Membrane ruffling was initiated in all 3 amoeboid PTC microglia tested.

These data suggest that 2MeSATP activates a distinct purinergic receptor, which is responsible for the effects of strong ADP stimuli. In experiments with specific P2Y receptor antagonists, we found that the P2Y6 antagonist MRS2578 (10 μM) did not

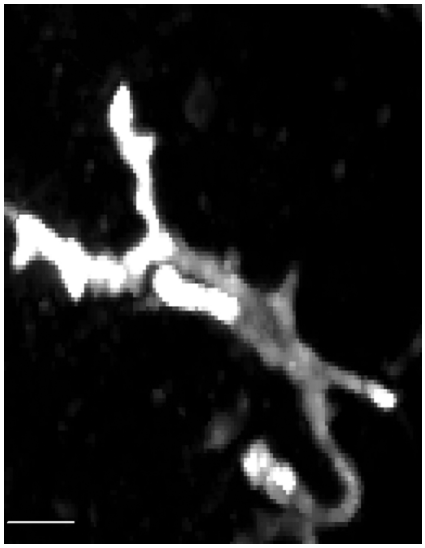

Movie 5. Joint application of P2Y1 (MRS2500, 10 μM) and P2Y13 (MRS2211, 30 μM) antagonists, at time counter = 11.00 min, suppresses ADP-induced (2 mM) process retraction of an initially ramified microglia from the dentate gyrus of an MTLE tissue. ADP applied at time counter = 30.00 min. Scale bar 10 μm, bottom left. Frame rate 3/s.

block the ADP 2 mM induced process retraction (4 ramified PTC cells; data not shown). The P2Y1 antagonists MRS2179 (5–10 μM) and MRS2500 (10 μM) did not suppress process withdrawal. A reduction of 33 ± 5% in mean cross-sectional area was induced by 2 mM ADP applied in the presence of the antagonists (p = 0.002; t = 6.50; n = 5, 3 MTLE and 2 PTC cells; Fig. 6*D*). The P2Y13 antagonist MRS2211 (10 μM) did not suppress ADP-mediated retraction of processes of ramified cells. Mean cross-sectional area was reduced by 31 ± 6% by 2 mM ADP application in the presence of MRS2211 (p = 0.01; t = 4.97; n = 4 PTC cells; Fig. 6*E*). Furthermore, membrane ruffling induced in amoeboid microglia by 2 mM ADP persisted in the presence of MRS2211 (n = 4 PTC cells).

However, joint application of P2Y1 and P2Y13 antagonists suppressed process retraction (MRS2500 and MRS2211; Fig. 6*F*,*G*; Movie 5). In the presence of both antagonists, mean cross-sectional area changed by only 5 ± 7% in response to 2 mM ADP (p = 0.18; t = 1.62; n = 5 ramified cells; 2 MTLE, 3 PTC microglia; Fig. 6*G*). In 3 of 5 initially ramified cells, some microglial processes retracted and others extended, but overall cross-sectional area was little changed. Microglial perisomatic volume tended to increase (Fig. 6*G*) and membrane ruffling was suppressed in the presence of both antagonists.

We next sought anatomical support for a possible role of P2Y1 and P2Y13 receptors in microglial process retraction using immunohistochemistry to test their expression in microglia. Microglia were identified by Iba1 immunostaining together with P2Y1 and P2Y13 receptor antibodies (see Materials and Methods). Expression was examined for 95 Iba1$^+$ cells (47 ramified, 48 amoeboid) in 6 PTC slices from 3 patients (Fig. 7). P2Y1$^+$ immunostained 70% of Iba1$^+$ cells (76% ramified, 62% amoeboid cells). P2Y13 immunopositivity was expressed by 63% of Iba1$^+$ cells (80% ramified, 45% amoeboid cells). Both P2Y1 and P2Y13 immunostaining was detected outside Iba1$^+$ cells, suggesting that other cell types may express these receptors.

Microglial process extension and retraction in response to neuronal ablation

Finally, we used laser ablation to examine the effects of tissue damage on the process motility of local microglia (Davalos et al., 2005; Eyo et al., 2014). Since damage induces purine release (possibly with other mediators), this approach let us test the legitimacy of pharmacological data. Bright-field images from targeted regions with initially visible neurons were examined before and after stimulation to monitor effects of laser ablation.

In response to laser damage, all microglia (4 amoeboid and 3 ramified PTC and MTLE cells) extended 1–3 novel processes. They projected 15–30 μm toward the damage site and encircled the damaged region (Fig. 8*A*; Movie 6). As in responses to ADP, the tips of extending processes terminated in bulbous endings. Phagocytic cup-like structures were sometimes apparent. Process extension was initiated at ~3 min after laser stimulation and ceased at ~10 min. Mean microglial cross-sectional area increased by 52 ± 14% (p = 0.01; t = −3.62; 7 PTC and MTLE cells). This convergence of extending microglial processes resembles responses to neuronal damage (Petersen and Dailey, 2004), NMDA receptor activation (Dissing-Olesen et al., 2014), or low calcium levels (Eyo et al., 2015).

We next examined the effects of the P2Y12 antagonist PSB0739 (1 μM) on process extension induced by laser damage (4 initially amoeboid cells PTC, 3 ramified cells, PTC). PSB0739 induced process retraction and membrane ruffling (as Fig. 5*B*). A further laser stimulation at the same site, in the presence of the antagonist, no longer triggered process extension, but rather retraction and membrane ruffling (4 amoeboid and 3 ramified cells, PTC; Fig. 8*B*; Movie 6).

If the P2Y12 antagonist suppresses process extension toward a damaged site, extension should be restored in its absence. We tested this point with a second stimulation at the same site with observations on 4 PTC and 2 MTLE cells. In response to the second laser stimulus, mean process cross-sectional area increased by 47 ± 18% (p = 0.04; t = −2.57; 4 PTC cells, 2 MTLE cells; Movie 7). The movie shows that processes with bulbous endings at their tips approach and encircle the damaged site.

Discussion

This work examined purinergic effects on processes of microglia from patients with MTLE and with glioma, both associated with an inflammatory state. Purines induced process extension at low doses and process retraction at higher doses. Process extension, for both ramified and amoeboid microglia, resulted from the activation of P2Y12 receptors. Laser-induced tissue damage reproduced microglial process extension. P2Y12 receptors also tonically promoted microglia process surveillance movements. Our data suggest that joint activation of P2Y1 and P2Y13 receptors underlies process retraction and ruffling behaviors initiated by higher-intensity purinergic stimuli.

Microglia in a pathological context: response to low- and high-intensity purinergic stimuli

Immunostaining showed most, possibly all, MTLE and PTC microglia expressed the P2Y12 receptor, which triggers process extension in rodents (Haynes et al., 2006; Ohsawa et al., 2010; Dissing-Olesen et al., 2014). A minority of microglia were immunopositive for the A2A receptor, which we supposed might initiate process retraction (Orr et al., 2009; Gyoneva et al., 2014). Motility responses were consistent with these data. Process extension by both ramified and amoeboid microglia initiated by weak purinergic stimuli was suppressed by antagonists of P2Y12 recep-

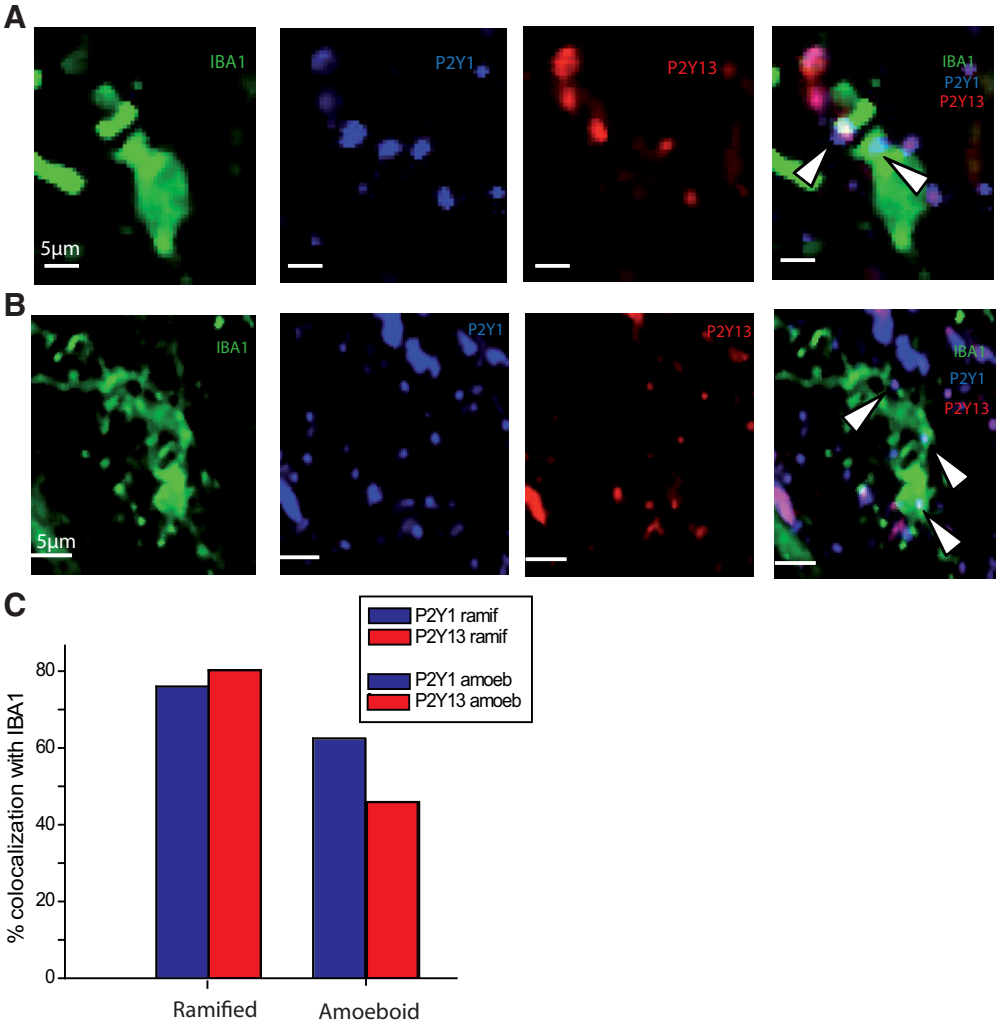

Figure 7. P2Y1 and P2Y13 immunostaining. ***A***, Immunostaining against P2Y1 and P2Y13 receptors in an IBA1^{+} microglia (amoeboid cell of PTC). ***B***, P2Y1 and P2Y13 receptor immunostaining for a ramified PTC cell. ***A***, ***B***, From left, Iba1 staining (green), P2Y1 staining (blue), P2Y13 staining (red), and merge of P2Y1, P2Y13, and Iba1 staining. Arrows indicate the spatial overlap of P2Y1 and P2Y13 staining in Iba1^{+} cells in both ***A*** and ***B***. Such overlap was seen in 47% (45 of 95) of Iba1^{+} microglia. ***C***, Ramified cells ($n = 47$) were more likely than amoeboid cells ($n = 48$) to be immunopositive for P2Y1 (blue) or P2Y13 receptors (red).

tors. Process retraction induced by stronger stimuli was not suppressed by A2A receptor antagonists but was blocked by joint application of P2Y1 and P2Y13 receptor antagonists.

In rodents, surveilling, ramified cells and amoeboid, "activated" microglia respond differently to purinergic stimuli. Microglia "activated" by LPS treatment retract, rather than extend, their processes. Microglial expression of P2Y12 receptors is downregulated after LPS treatment (Haynes et al., 2006; Orr et al., 2009). A2A receptors are upregulated and trigger retraction (Orr et al., 2009; Gyoneva et al., 2014). Our data show that microglia in tissue from patients with MTLE or gliomas do not behave in this way.

How similar are the phenotypes of "activated" human epileptic microglia and LPS-treated rodent cells? Microglia of epileptic human tissue were first classed as

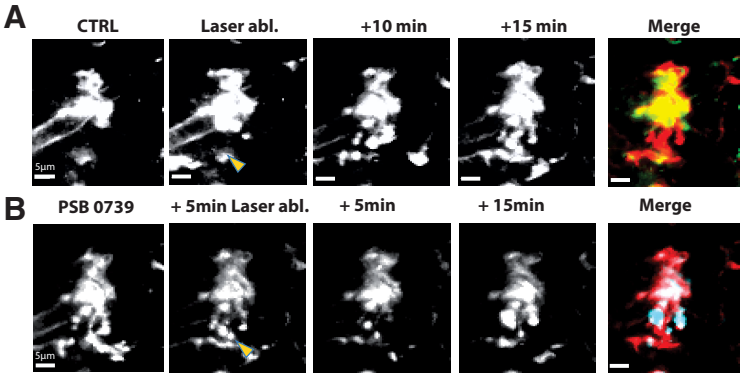

Figure 8. Role of P2Y receptors in microglial motility induced by tissue damage. ***A***, The effects of local laser stimulation. Control images of an initially amoeboid cell from PTC before (CTRL), immediately after laser damage (yellow arrow), and at 10 and 15 min later. Merge is the difference between control and 15 min images. Red represents new membrane signal. Green represents lost signal. ***B***, The same cell after a second laser stimulus (yellow arrow) applied 5 min after the P2Y12 antagonist PSB0739 (1 μM). Images are shown at 5 and 15 min after stimulation. Merge is the difference between PSB0739 and 15 min images. Red represents lost membrane signal due to process retraction. Blue represents new membrane signal from ruffling. Movie 6 shows that local laser damage induces process extension and is blocked by P2Y12R antagonist. Movie 7 shows that process extension is restored in the absence of P2Y12R antagonist.

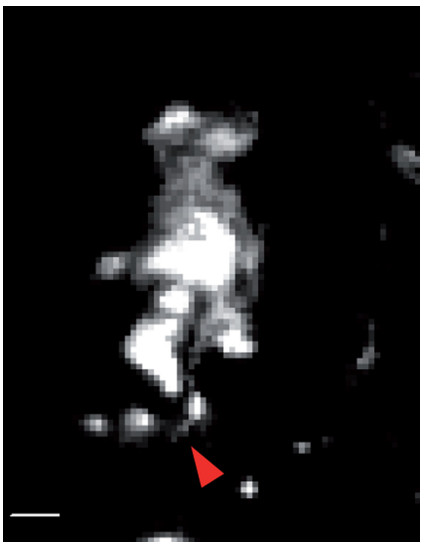

Movie 6. Laser-induced tissue damage induces process extension by an initially amoeboid microglia of PTC. Red circle represents laser damage. First laser stimulus at time counter = 2.59 min. PSB0739 (1 μM) was applied at time counter = 16.59 min. Second laser stimulus of the same intensity at the same site, at time counter = 21.59 min. Scale bar 10 μm, bottom left. Frame rate 3/s.

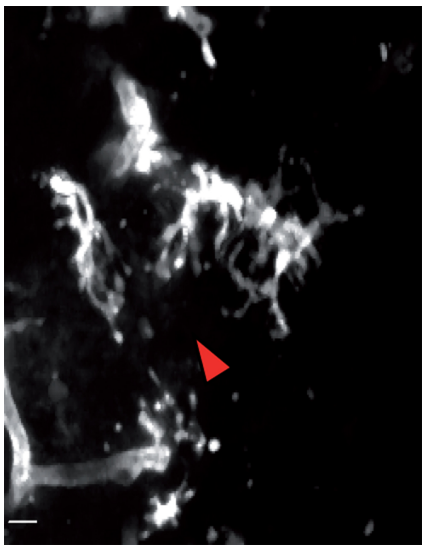

Movie 7. Two laser stimuli at interval of 7 min both induce process extension by 2 initially amoeboid and 1 ramified microglia of PTC. Green arrow indicates the targeted region. Red circle represents the visible extent of damage. First laser stimulation at time 3.00 min and the second at time counter 10.37 min. Scale bar 10 μm, bottom left. Frame rate 3/s.

"reactive" according to shape and inflammatory marker expression (Beach et al., 1995). We now know that seizures release inflammatory molecules (Vezzani et al., 1999; Morin-Brureau et al., 2018) and rupture the blood–brain barrier (Cornford, 1999; Cacheaux et al., 2009), permitting entry of systemic immune cells. Our data showed that microglia of the CA1 region in MTLE tissue or closer to the tumor in PTC tissue were more likely to possess an "activated" shape with few or no processes. However, P2Y12 receptor expression by cells of all shapes (Fig. 4) seems inconsistent with other human data. Microglia close to lesions in tissue of multiple sclerosis patients (Mildner et al., 2017; Zrzavy et al., 2017) or near-amyloid tangles in patients with Alzheimer's disease (Mildner et al., 2017) show little or no P2Y12 immunostaining. We note that the antibody used here recognizes the same 40-amino acid cytoplasmic region of the receptor as that used by Mildner et al. (2017). Data showing all Iba1$^+$ elements were P2Y12$^+$ (compare Mildner et al., 2017) suggest that cells studied here were microglia rather than infiltrating immune cells.

However microglia "activated" in different contexts may exhibit distinct motility patterns and express different receptors. "Alternatively activated" human microglia, treated with interleukins IL-4 and IL13 rather than LPS, show more intense immunostaining against P2Y12 and respond more strongly to ADP (Moore et al., 2015). "Alternatively activated" microglia are linked to repair processes, as transcriptomic data from the CA1 region of MTLE tissue suggest (Morin-Brureau et al., 2018). In kainate-treated epileptic mice, "activated" microglia continue to extend processes toward purinergic stimuli or cellular damage (Avignone et al., 2015). The phenotype of "activated" microglia in human epileptic brain may not be identical to that of LPS-treated rodent cells.

P2Y12R: microglial process extension and basal effects on surveillance

We found few differences between ramified and amoeboid microglia in the process extension induced by low-intensity purinergic stimuli (Haynes et al., 2006; Ohsawa et al., 2010; Dissing-Olesen et al., 2014). Increases in cross-sectional area were large, 80%–100% for initially amoeboid cells, possibly mediated by endocytic membrane recycling (Kay et al., 2008). Processes were directed toward purinergic stimuli, and P2Y12 receptors moved toward growth sites (Dissing-Olesen et al., 2014). Microglia of MTLE and PTC tissue exhibited similar motility responses. Similarly, even though ambient glutamate levels in PTC are higher than in MTLE tissue (Buckingham et al., 2011) and mitosis and cell cycle-related molecules are upregulated in peritumoral microglia (Szulzewsky et al., 2016), specific tumor-associated macrophages may have immunosuppressive effects in glioblastoma (Chen and Hambardzumyan, 2018), and immune-related transcripts of human microglia (Szulzewsky et al., 2016) are not notably upregulated in glioblastoma tissue.

Actions of the antagonists PSB0739 and Ticagrelor suggest that tonic activation of the P2Y12 receptor promotes nondirected surveillance movements. Similar conclusions have emerged from work on spinal microglia of mice genetically deficient for the P2Y12 receptor (Gu et al., 2016), but not from rodent hippocampal microglia treated with receptor antagonists (Madry et al., 2018). A role for P2Y12 receptors in directed extension of rodent microglial processes is generally agreed (Haynes et al., 2006; Madry et al., 2018), although adenosine receptors may also need to be activated (Matyash et al., 2017). Pathways linking P2Y12 receptor activation to process extension remain to be completely described. This receptor is coupled to $G_{\alpha i}$ (Erb and Weisman, 2012; Abbracchio et al., 2019). Activation inhibits adenylate cyclase, increases internal Ca, and induces K-currents. Those mediated by the 2-pore channel, THIK1, contribute to surveillance movements but not process extension (Madry et al., 2018). Akt, a Ca-dependent kinase, activates beta1 integrins facilitating process extension by interactions with the extracellular matrix (Somanath et al., 2007; Ohsawa et al., 2010). The PI3k pathway has been implicated in purine-induced chemotaxis (Wu et al., 2007). Small GTPase pathways are crucial modulators of cytoskeletal actin remodeling (Sadok and Marshall, 2014; Rottner et al.,

2017), but their involvement in microglial process extension is not clear.

P2Y1/P2Y13: joint effects on microglial process retraction and ruffling

Our data suggest that P2Y1 and P2Y13 receptors are involved in microglial process retraction induced by high-dose purinergic stimuli, the same as used previously in rodents (Eyo et al., 2014; Madry et al., 2018). Ramified cells of both MTLE and PTC behaved similarly. In contrast to extension, which was directed, retraction was nondirectional. Membrane ruffling of ramified and amoeboid cells, induced by high-intensity stimuli, was also suppressed by simultaneously applied P2Y1 and P2Y13 antagonists.

Neither P2Y1 nor P2Y13 receptors have been linked to microglial process retraction. The P2Y1 receptor is coupled to $G_{\alpha q}$ and activates phospholipase C as well as the small GTPases Rac and Rho (Erb and Weisman, 2012; Abbracchio et al., 2019). The P2Y13 receptor is strongly homologous to P2Y12, coupled to the same $G_{\alpha i}$ and also inhibits adenylate cyclase as well as RhoA, a small GTPase. Links between P2Y1 and P2Y13 receptors, actin filament remodeling, and process retraction remain to be explored.

The finding that both P2Y1 and P2Y13 antagonists were needed to suppress process retraction might imply a synergy between signaling pathways initiated by distinct receptors or rather reflect the activation of a single receptor entity. Precedents exist for either possibility. For instance, there is reciprocal cross talk between intracellular pathways activated by P2Y1 and P2Y12 receptors in platelets (Hardy et al., 2004). Alternatively, distinct G-protein-coupled receptors may express as dimers (Gurevich and Gurevich, 2008). P2Y1 receptors form heteromers with both P2Y11 (Ecke et al., 2008) and A1R adenosine receptors (Yoshioka et al., 2001). Immunostaining data (Fig. 7) suggested that P2Y1 and P2Y13 were expressed at higher levels in ramified than amoeboid microglia but not universally, unlike P2Y12 receptors. Staining could seem to overlap on Iba1$^+$ cells, raising the possibility that both antibodies recognized receptors involved in retraction.

Functional significance

Our data on microglial process movements induced by focal tissue damage reinforce results from purine applications, although we did not measure levels of purines or adenosine (Llaudet et al., 2005). Epileptiform activity induced in slices causes adenosine increases in the range of 10 μM with smaller changes in ATP (Frenguelli and Wall, 2016). Extracellular purine levels may be much higher after brain damage in part due to ATP release from astrocytes (Franke et al., 2006; Choo et al., 2013).

Microglia adopt shapes ranging from "reactive" ovoid cells through "activated" microglia with large soma and some thick processes to highly ramified cells (Fig. 9). We suggest that purinergic signaling could partially, but not completely, underlie cycling of a given cell through these different shapes and back again (Hanisch and Kettenmann, 2007; Jonas et al., 2012; Yamada and Jinno, 2013). Specifically, weak ADP stimuli and cell damage induce strong process extension by amoeboid or even round microglia. However, process retraction of highly ramified cells exposed to high purine levels does not produce completely amoeboid cells, but rather microglia with shorter ramifications.

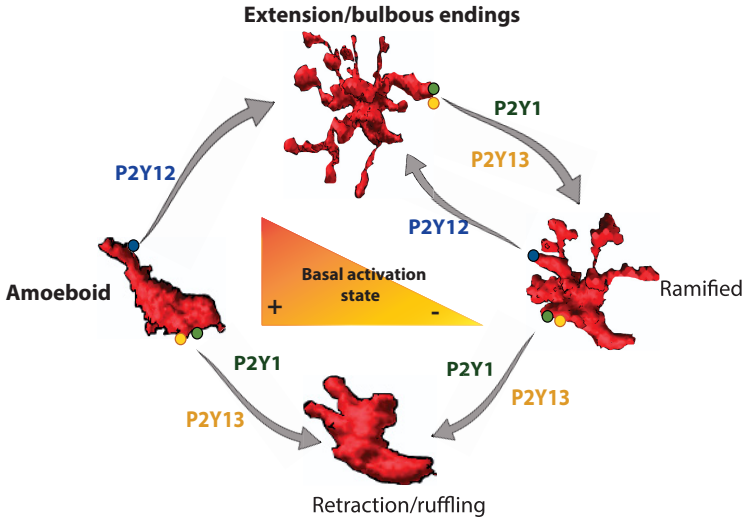

Figure 9. Schema of microglial shape changes and P2Y receptors. Amoeboid and ramified cells are basal microglial states. Microglia change shape between states accordingly to levels of ATP/ADP.

In conclusion, we have implemented live imaging of microglia in tissue from patients with temporal lobe epilepsy and cortical glioma. Cell shape varied from highly ramified microglia to cells with few or no processes. Low levels of purinergic stimuli intensity induced process extension of all microglia mediated via P2Y12 receptors. Higher purine doses induced retraction of ramified microglial processes and membrane ruffling, which were suppressed by joint application of P2Y1 and P2Y13 receptor antagonists.

References

Abbracchio MP, Jacobson KA, Burnstock G, Boeynaems JM, Ceruti S, Fumagalli M, Gachet C, Kennedy C, King BF, Lecca D, Weisman GA, Boyer JL, Humphries RG, Inoue K, Miras-Portugal MT, Ralevic V, Hills R (2019) P2Y receptors. In: IUPHAR/BPS guide to pharmacology. Accessed July 31, 2019. Available at http://www.guidetopharmacology.org/GRAC/FamilyDisplayForward?familyId=52.

Acarin L, Vela JM, González B, Castellano B (1994) Demonstration of poly-N-acetyl lactosamine residues in ameboid and ramified microglial cells in rat brain by tomato lectin binding. J Histochem Cytochem 42:1033–1041.

Avignone E, Lepleux M, Angibaud J, Nägerl UV (2015) Altered morphological dynamics of activated microglia after induction of status epilepticus. J Neuroinflammation 12:202–215.

Baqi Y, Atzler K, Köse M, Glänzel M, Müller CE (2009) High-affinity, non-nucleotide-derived competitive antagonists of platelet P2Y12 receptors. J Med Chem 52:3784–3793.

Beach TG, Woodhurst WB, MacDonald DB, Jones MW (1995) Reactive microglia in hippocampal sclerosis associated with human temporal lobe epilepsy. Neurosci Lett 191:27–30.

Bianco F, Pravettoni E, Colombo A, Schenk U, Möller T, Matteoli M, Verderio C (2005) Astrocyte-derived ATP induces vesicle shedding and IL-1β release from microglia. J Immunol 174:7268–7277.

Blümcke I, Thom M, Aronica E, Armstrong DD, Bartolomei F, Bernasconi A Bernasconi N, Bien CG, Cendes F, Coras R, Cross JH, Jacques TS, Kahane P, Mathern GW, Miyata H, Moshé SL, Oz B, Özkara C, Perucca E, Sisodiya S, et al. (2013) International consensus classification of hippocampal sclerosis in temporal lobe epilepsy: a task force report from the ILAE commission on diagnostic methods. Epilepsia 54:1315–1329.

Boche D, Perry VH, Nicoll JA (2013) Activation patterns of microglia and their identification in the human brain. Neuropathol Appl Neurobiol 39:3–18.

Bordey A, Spencer DD (2003) Chemokine modulation of high-conductance Ca^{++}-sensitive K^+ currents in microglia from human hippocampi. Eur J Neurosci 18:2893–2898.

Boya J, Calvo JL, Carbonell AL, Borregon A (1991) A lectin histochemistry study on the development of rat microglial cells. J Anat 175:229–236.

Buckingham SC, Robel S (2013) Glutamate and tumor-associated epilepsy: glial cell dysfunction in the peritumoral environment. Neurochem Int 63:696–701.

Buckingham SC, Campbell SL, Haas BR, Montana V, Robel S, Ogunrinu T, Sontheimer H (2011) Glutamate release by primary brain tumors induces epileptic activity. Nat Med 17:1269–1274.

Cacheaux LP, Ivens S, David Y, Lakhter AJ, Bar-Klein G, Shapira M, Heinemann U, Friedman A, Kaufer D (2009) Transcriptome profiling reveals TGF-beta signaling involvement in epileptogenesis. J Neurosci 29:8927–8935.

Cattaneo M (2010) New P2Y(12) inhibitors. Circulation 121:171–179.

Chen JF, Lee CF, Chern Y (2014) Adenosine receptor neurobiology: overview. Int Rev Neurobiol 119:1–49.

Chen Z, Hambardzumyan D (2018) Immune microenvironment in glioblastoma subtypes. Front Immunol 9:1004.

Choo AM, Miller WJ, Chen YC, Nibley P, Patel TP, Goletiani C, Morrison B 3rd, Kutzing MK, Firestein BL, Sul JY, Haydon PG, Meaney DF (2013) Antagonism of purinergic signalling improves recovery from traumatic brain injury. Brain 136:65–80.

Cornford EM (1999) Epilepsy and the blood brain barrier: endothelial cell responses to seizures. Adv Neurol 79:845–862.

Dailey ME, Waite M (1999) Confocal imaging of microglial cell dynamics in hippocampal slice cultures. Methods 18:222–230.

Dale N (1998) Delayed production of adenosine underlies temporal modulation of swimming in frog embryo. J Physiol 511:265–272.

Dale N, Frenguelli BG (2009) Release of adenosine and ATP during ischemia and epilepsy. Curr Neuropharmacol 7:160–179.

Davalos D, Grutzendler J, Yang G, Kim JV, Zuo Y, Jung S, Littman DR, Dustin ML, Gan WB (2005) ATP mediates rapid microglial response to local brain injury in vivo. Nat Neurosci 8:752–758.

Davis EJ, Foster TD, Thomas WE (1994) Cellular forms and functions of brain microglia. Brain Res Bull 34:73–78.

Dissing-Olesen L, MacVicar BA (2015) Fixation and immunolabeling of brain slices: SNAPSHOT method. Curr Protoc Neurosci 71:1.23.1–1.23.12.

Dissing-Olesen L, LeDue JM, Rungta RL, Hefendehl JK, Choi HB, MacVicar BA (2014) Activation of neuronal NMDA receptors triggers transient ATP-mediated microglial process outgrowth. J Neurosci 34:10511–10527.

Ecke D, Hanck T, Tulapurkar ME, Schäfer R, Kassack M, Stricker R, Reiser G (2008) Hetero-oligomerization of the P2Y11 receptor with the P2Y1 receptor controls the internalization and ligand selectivity of the P2Y11 receptor. Biochem J 409:107–116.

Erb L, Weisman GA (2012) Coupling of P2Y receptors to G proteins and other signaling pathways. Interdiscip Rev Membr Transp Signal 1:789–803.

Eyo UB, Peng J, Swiatkowski P, Mukherjee A, Bispo A, Wu LJ (2014) Neuronal hyperactivity recruits microglial processes via neuronal NMDA receptors and microglial P2Y12 receptors after status epilepticus. J Neurosci 34:10528–10540.

Eyo UB, Gu N, De S, Dong H, Richardson JR, Wu LJ (2015) Modulation of microglial process convergence toward neuronal dendrites by extracellular calcium. J Neurosci 35:2417–2422.

Franke H, Krügel U, Illes P (2006) P2 receptors and neuronal injury. Pflugers Arch 452:622–644.

Frenguelli BG, Wall MJ (2016) Combined electrophysiological and biosensor approaches to study purinergic regulation of epileptiform activity in cortical tissue. J Neurosci Methods 260:202–214.

Gu N, Eyo UB, Murugan M, Peng J, Matta S, Dong H, Wu LJ (2016) Microglial P2Y12 receptors regulate microglial activation and surveillance during neuropathic pain. Brain Behav Immun 55:82–92.

Gurevich VV, Gurevich EV (2008) How and why do GPCRs dimerize? Trends Pharmacol Sci 29:234–240.

Gyoneva S, Davalos D, Biswas D, Swanger SA, Garnier-Amblard E, Loth F, Akassoglou K, Traynelis SF (2014) Systemic inflammation regulate microglial response to tissue damage in vivo. Glia 62:1345–1360.

Hanisch UK, Kettenmann H (2007) Microglia: active sensor and versatile effector cells in the normal and pathologic brain. Nat Neurosci 10:1387–1394.

Hardy AR, Jones ML, Mundell SJ, Poole AW (2004) Reciprocal cross-talk between P2Y1 and P2Y12 receptors at the level of calcium signaling in human platelets. Blood 104:1745–1752.

Haynes SE, Hollopeter G, Yang G, Kurpius D, Dailey ME, Gan WB, Julius D (2006) The P2Y12 receptor regulates microglial activation by extracellular nucleotides. Nat Neurosci 9:1512–1519.

Honda S, Sasaki Y, Ohsawa K, Imai Y, Nakamura Y, Inoue K, Kohsaka S (2001) Extracellular ATP or ADP induce chemotaxis of cultured microglia through Gi/o-coupled P2Y receptors. J Neurosci 21:1975–1982.

Huberfeld G, Menendez de la Prida L, Pallud J, Cohen I, Le Van Quyen M, Adam C, Clemenceau S, Baulac M, Miles R (2011) Glutamatergic preictal discharges emerge at the transition to seizure in human epilepsy. Nat Neurosci 14:627–634.

Jonas RA, Yuan TF, Liang YX, Jonas JB, Tay DK, Ellis-Behnke RG (2012) The spider effect: morphological and orienting classification of microglia in response to stimuli in vivo. PLoS One 7:e30763.

Kay RR, Langridge P, Traynor D, Hoeller O (2008) Changing directions in the study of chemotaxis. Nat Rev Mol Cell Biol 9:455–463.

Khakh BS, North RA (2012) Neuromodulation by extracellular ATP and P2X receptors in the CNS. Neuron 76:51–69.

Kim YC, Lee JS, Sak K, Marteau F, Mamedova L, Boeynaems JM, Jacobson KA (2005) Synthesis of pyridoxal phosphate derivatives with antagonist activity at the P2Y13 receptor. Biochem Pharmacol 70:266–274.

Koizumi S, Shigemoto-Mogami Y, Nasu-Tada K, Shinozaki Y, Ohsawa K, Tsuda M, Joshi BV, Jacobson KA, Kohsaka S, Inoue K (2007) UDP acting at P2Y6 receptors is a mediator of microglial phagocytosis. Nature 446:1091–1095.

Le Duigou C, Savary E, Morin-Brureau M, Gomez-Dominguez D, Sobczyk A, Chali F, Milior G, Kraus L, Meier JC, Kullmann DM, Mathon B, de la Prida LM, Dorfmuller G, Pallud J, Eugène E, Clemenceau S, Miles R (2018) Imaging pathological activities of human brain tissue in organotypic culture. J Neurosci Methods 298:33–44.

Llaudet E, Hatz S, Droniou M, Dale N (2005) Microelectrode biosensor for real-time measurement of ATP in biological tissue. Anal Chem 77:3267–3273.

Madry C, Kyrargyri V, Arancibia-Cárcamo IL, Jolivet R, Kohsaka S, Bryan RM, Attwell D (2018) Microglial ramification, surveillance, and interleukin-1β release are regulated by the two-pore domain K^+ channel THIK-1. Neuron 97:299–312.e6.

Matyash M, Zabiegalov O, Wendt S, Matyash V, Kettenmann H (2017) The adenosine generating enzymes CD39/CD73 control microglial processes ramification in the mouse brain. PLoS One 12:e0175012.

Mildner A, Huang H, Radke J, Stenzel W, Priller J (2017) P2Y12 receptor is expressed on human microglia under physiological conditions throughout development and is sensitive to neuroinflammatory diseases. Glia 65:375–387.

Moore CS, Ase AR, Kinsara A, Rao VT, Michell-Robinson M, Leong SY, Butovsky O, Ludwin SK, Séguéla P, Bar-Or A, Antel JP (2015) P2Y12 expression and function in alternatively activated human microglia. Neurol Neuroimmunol Neuroinflamm 2:e80.

Morin-Brureau M, Milior G, Royer J, Chali F, LeDuigou C, Savary E, Blugeon C, Jourdren L, Akbar D, Dupont S, Navarro V, Baulac M, Bielle F, Mathon B, Clemenceau S, Miles R (2018) Microglial phenotypes in the human epileptic temporal lobe. Brain 41:3343–3360.

Neustadt BR, Liu H, Hao J, Greenlee WJ, Stamford AW, Foster C, Arik L, Lachowicz J, Zhang H, Bertorelli R, Fredduzzi S, Varty G, Cohen-Williams M, Ng K (2009) Potent and selective adenosine A2A receptor antagonists: 1,2,4-triazolo[1,5-c]pyrimidines. Bioorg Med Chem Lett 19:967–971.

Nimmerjahn A, Kirchhoff F, Helmchen F (2005) Resting microglial cells are highly dynamic surveillants of brain parenchyma in vivo. Science 308:1314–1318.

Ohsawa K, Irino Y, Sanagi T, Nakamura Y, Suzuki E, Inoue K, Kohsaka S (2010) P2Y12 receptor-mediated integrin-beta1 activation regulates microglial process extension induced by ATP. Glia 58:790–801.

Orr AG, Orr AL, Li XJ, Gross RE, Traynelis SF (2009) Adenosine A(2A) receptor mediates microglial process retraction. Nat Neurosci 12:872–878.

Pallud J, Le Van Quyen M, Bielle F, Pellegrino C, Varlet P, Cresto N, Baulac M, Duyckaerts C, Kourdougli N, Chazal G, Devaux B, Rivera C, Miles R, Capelle L, Huberfeld G (2014) Cortical GABA-ergic excitation contributes to epileptic activities around human glioma. Sci Transl Med. 6:244ra89.

Paolicelli RC, Bolasco G, Pagani F, Maggi L, Scianni M, Panzanelli P, Giustetto M, Ferreira TA, Guiducci E, Dumas L, Ragozzino D, Gross CT (2011) Synaptic pruning by microglia is necessary for normal brain development. Science 333:1456–1458.

Pelegrin P, Barroso-Gutierrez C, Surprenant A (2008) P2X7 receptor differentially couples to distinct release pathways for IL-1beta in mouse macrophage. J Immunol 180:7147–7157.

Petersen MA, Dailey ME (2004) Diverse microglial motility behaviors during clearance of dead cells in hippocampal slices. Glia 46:195–206.

Quintas C, Vale N, Gonçalves J, Queiroz G (2018) Microglia P2Y13 receptors prevent astrocyte proliferation mediated by P2Y1 receptors. Front Pharmacol 9:418.

Raposo C, Schwartz M (2014) Glial scar and immune cell involvement in tissue remodeling and repair following acute CNS injuries. Glia 62:1895–1904.

Ravizza T, Gagliardi B, Noé F, Boer K, Aronica E, Vezzani A (2008) Innate and adaptive immunity during epileptogenesis and spontaneous seizures: evidence from experimental models and human temporal lobe epilepsy. Neurobiol Dis 29:142–160.

Riegel AK, Faigle M, Zug S, Rosenberger P, Robaye B, Boeynaems JM, Idzko M, Eltzschig HK (2011) Selective induction of endothelial P2Y6 nucleotide receptor promotes vascular inflammation. Blood 117:2548–2555.

Rottner K, Faix J, Bogdan S, Linder S, Kerkhoff E (2017) Actin assembly mechanisms at a glance. J Cell Sci 130:3427–3435.

Sadok A, Marshall CJ (2014) Rho GTPases, small GTPases. 5:e983878.

Sanz JM, Di Virgilio F (2000) Kinetics and mechanism of ATP-dependent IL-1β release from microglial cells. J Immunol 164:4893–4898.

Schafer DP, Lehrman EK, Kautzman AG, Koyama R, Mardinly AR, Yamasaki R, Ransohoff RM, Greenberg ME, Barres BA, Stevens B (2012) Microglia sculpt postnatal neural circuits in an activity and complement-dependent manner. Neuron 74:691–705.

Schwendele B, Brawek B, Hermes M, Garaschuk O (2012) High-resolution in vivo imaging of microglia using a versatile nongenetically encoded marker. Eur J Immunol 42:2193–2196.

Shinozaki Y, Nomura M, Iwatsuki K, Moriyama Y, Gachet C, Koizumi S (2014) Microglia trigger astrocyte-mediated neuroprotection via purinergic gliotransmission. Sci Rep 4:4329.

Somanath PR, Kandel ES, Hay N, Byzova TV (2007) Akt1 signaling regulates integrin activation, matrix recognition, and fibronectin assembly. J Biol Chem 282:22964–22976.

Streit WJ, Graeber MB, Kreutzberg GW (1988) Functional plasticity of microglia: a review. Glia 1:301–307.

Szulzewsky F, Arora S, de Witte L, Ulas T, Markovic D, Schultze JL, Holland EC, Synowitz M, Wolf SA, Kettenmann H (2016) Human glioblastoma-associated microglia/monocytes express a distinct RNA profile compared to human control and murine samples. Glia 64:1416–1436.

Varvel NH, Neher JJ, Bosch A, Wang W, Ransohoff RM, Miller RJ, Dingledine R (2016) Infiltrating monocytes promote brain inflammation and exacerbate neuronal damage after status epilepticus. Proc Natl Acad Sci U S A 113:E5665–E5674.

Vezzani A, Conti M, De Luigi A, Ravizza T, Moneta D, Marchesi F, De Simoni MG (1999) Interleukin-1beta immunoreactivity and microglia are enhanced in the rat hippocampus by focal kainate application: functional evidence for enhancement of electrographic seizures. J Neurosci 19:5054–5065.

von Kügelgen I (2006) Pharmacological profiles of cloned mammalian P2Y-receptor subtypes. Pharmacol Ther 110:415–432.

Wu LJ, Vadakkan KI, Zhuo M (2007) ATP-induced chemotaxis of microglial processes requires P2Y receptor-activated initiation of outward potassium currents. Glia 55:810–821.

Yamada J, Jinno S (2013) Novel objective classification of reactive microglia following hypoglossal axotomy using hierarchical cluster analysis. J Comp Neurol 521:1184–1201.

Yegutkin GG (2014) Enzymes involved in metabolism of extracellular nucleotides and nucleosides: functional implications and measurement of activities. Crit Rev Biochem Mol Biol 49:473–497.

Yoshioka K, Saitoh O, Nakata H (2001) Heteromeric association creates a P2Y-like adenosine receptor. Proc Natl Acad Sci U S A 98:7617–7622.

Zrzavy T, Hametner S, Wimmer I, Butovsky O, Weiner HL, Lassmann H (2017) Loss of 'homeostatic' microglia and patterns of their activation in active multiple sclerosis. Brain 140:1900–1913.